#420

ESRO-4

POSITIVE ION DATA

72-092A-01A

ESRO-4

POS. ION DATA, TAPE

72-092A-01A

THIS DATA SET HAS BEEN RESTORED. ORIGINALLY IT CONTAINED THREE 9-TRACK, 1600 BPI TAPES WRITTEN IN BINARY. THERE IS ONE RESTORED TAPE. THE DR TAPE IS 3480 CARTRIDGE AND THE DS TAPE IS 9-TRACK, 6250 BPI. THE ORIGINAL TAPES WERE CREATED ON AN IBM 360/65 COMPUTER AND WERE RESTORED ON THE MRS COMPUTER. THE DR AND DS NUMBERS ALONG WITH THE CORRESPONDING D NUMBERS AND TIME SPANS ARE AS FOLLOWS:

DR#	DS#	D#	FILES	TIME SPAN
DR005273	DS005273	D030957	1	11/22/72 - 05/10/73
		D030958	2	05/11/73 - 11/04/73
		D030959	3	11/04/73 - 04/14/74

REQ. AGENT	RAND NO.	ACQ. AGENT
CMP	RC9052	RNH

ESRO-4

POSITIVE ION DATA

72-092A-01A

This data set catalog contains 3 tapes. They are 9 track, Binary, 1600 BPI, and created on an IBM 360/65 computer. Also included in this catalog is a listing supplied by the experimenter of D-30957. Each tape has 1 file. The tape format is on page VI-2 of the Post Launch Report.

D#	C#	TIME SPAN
D-30957	C-19813	11/22/72 - 05/10/73
D-30958	C-19814	07/17/73 - 11/04/73
D-30959	C-19185	11/04/73 - 04/14/74

72 - 092A - 01

ESRO-4 EXPERIMENT

S45

TECHNICAL DESCRIPTION

MULLARD SPACE SCIENCE LABORATORY
UNIVERSITY COLLEGE LONDON

EXPERIMENT S45 TO BE FLOWN ON ESRO SATELLITE ESRO - 4

An experiment to measure the structure of the major ionic species in the topside ionosphere over a height range of 350 - 1000 km at latitudes from - 90^{o} to + 90^{o} geographic.

W.J. Raitt
Mullard Space Science Laboratory
University College London
April, 1970

Table of Contents

1. Purpose of Experiment

The purpose of the experiment is to investigate the properties of the major ion species of the topside ionosphere with particular attention to ionic species, energy distribution and drift velocity. The main sensor will be backed up by other sensors to assist in the analysis, and as a by-product these other sensors will provide information on electron temperature, electron density and irregularities in the total ion density as small as a change of 0.5%.

2. Method Used

All of the sensors referred to above will consist of electrodes immersed in the ionospheric plasma attached to suitable electronic analysers so that functions of the current flowing to the electrodes in terms of the voltage applied to them may be studied. This type of sensor is known as the Langmuir probe after the American physicist Irving Langmuir (1926) who did much to develop both the theoretical and practical aspects of probes during the 1920's and 1930's.

The biasing voltages for the electrodes are chosen so that measurements may be made on both negative and positive charge carriers.

The main sensor consists of a large, spherical ion collecting probe of 19 cms diameter. This is supplemented by an electron collecting spherical probe to ascertain vehicle potential, and a spherical probe monitoring total ion current mounted on the spin axis of the vehicle to avoid spin modulation effects on this current.

3. Outline of Theory

The work of Langmuir has been extended by Medicus (1961, 1962) who has, in particular, applied the theory to the case of a plasma consisting of ions having a Maxwellian velocity distribution due to their temperature superimposed on a steady drift velocity. This is, in fact, the situation applicable to a probe mounted on a spacecraft, the drift velocity being the spacecraft velocity relative to the plasma.

3.1. Spherical ion probe

This probe will be referred to henceforth as a mass spectrometer because of its ability to resolve different ion species. This may be understood qualitatively by considering that an ion of species i will have an energy in the frame of reference of the spacecraft of

$$E_i = \tfrac{1}{2} m_i V_s^2 \quad \ldots\ldots\ldots\ldots\ldots\ldots\ldots (1)$$

where V_s is the spacecraft velocity.

Thus, in order to prevent ions of this species reaching the probe, a voltage V given by

$$eV_i = \tfrac{1}{2} m_i V_s^2 \quad \ldots\ldots\ldots\ldots\ldots\ldots\ldots (2)$$

must be applied to the probe.

Thus, in principle, by observing discontinuities in the current collected by the probe as the applied voltage is changed, the presence of various species may be detected. In practice, the ions have a random velocity distribution superimposed on this drift so the discontinuities are not sharp; however, provided

$$V_t \ll V_D$$

the discontinuities can be separated, where V_t = thermal vel.

V_D = drift vel.

It can be seen that this is a positive voltage, therefore to prevent the ion current being swamped by an electron current a grid biased to a negative potential must surround the probe surface. It can be shown from considerations of the conservation of angular momentum, that as far as the ion current collected by a spherical probe is concerned the grid has no effect other than to introduce a transparency factor.

Druyvesteyn (1930) has shown that the energy distribution of the ions is related to the current J collected by a Langmuir probe at potential V is given by

$$N(V)\, dV = \frac{d^2J}{dV^2} \Big/ V^{\frac{1}{2}} \quad \ldots\ldots\ldots\ldots\ldots\ldots\ldots (3)$$

where N(V) is the number of particles having energy $V \rightarrow V + dV$

Medicus (1962) gives the expression

$$\frac{d^2J}{d\eta^2} = K\left[\frac{\exp(-\eta-\eta_o)\sinh\left(2(\eta\eta_o)^{\frac{1}{2}}\right)}{(\pi\eta\eta_o)^{\frac{1}{2}}}\right] \quad \ldots\ldots\ldots \quad (4)$$

where $\eta = V/kT$

$\eta_o = V_o/kT$

$K = \pi e n\left(\frac{2kT}{m}\right)^{\frac{1}{2}} \cdot r^2$

e = electron charge

n = ion density

m = ion mass

r = probe radius

V_o = drift energy of ion species when thermal velocity is zero

T = ion temperature.

This expression is for one ion species assuming a Maxwellian velocity distribution.

If we write

$$S_i(\eta) = \frac{\exp(-\eta-\eta_{oi})\sinh\left(2(\eta\eta_{oi})^{\frac{1}{2}}\right)}{\eta^{\frac{1}{2}}} \quad \ldots\ldots\ldots \quad (5)$$

We can write the second derivative of current as a function of voltage for the ith species as

$$\left(\frac{d^2J}{dV^2}\right)_i = \frac{nAe}{kT\, m_i V_s \pi^{\frac{1}{2}}} S_i(\eta) \quad \ldots\ldots\ldots\ldots\ldots \quad (6)$$

where $A = \pi r^2$

Thus, if there are P ion species of fraction fi

$$\frac{d^2J}{dV^2} = \frac{nAe}{km_p V_s \pi^{\frac{1}{2}}} \cdot \frac{1}{T} \cdot \sum_{i=1}^{P} \frac{fi}{M_i} S_i(\eta) \quad \ldots\ldots\ldots \quad (7)$$

where m_p = proton mass

M_i = mass number of ith species.

Theoretical curves for this function have been evaluated and are shown in fig. 1.

It can be seen from the diagram that for the ion species expected in the topside F-region identification can be made, but complete resolution of

H^+ and He^+ is not possible. However, the resolution of the instrument should be sufficiently high for the two peaks to be distinguished in most of the circumstances when both H^+ and He^+ ions are present.

For the peak of a given ion species we have the relations:

$$V_m = f_1 (V_s, M_i, T_i)$$

$$W = f_2 (V_s, M_i, T_i)$$

$$A = f_3 (V_s, M_i, T_i, n_i)$$

where

V_m = Voltage at which peak maximum occurs
W = Width of peak at say half amplitude
A = Amplitude of peak

In fact V_m varies rather slowly with T_i and since the major ions present in the F-region are known to be H^+, He^+ or O^+ this provides a positive identification of M_i providing the potential of the vehicle relative to the ambient plasma is known. Having determined M_i T_i can be found from W and then n_i from A.

The functions f_1, f_2 and f_3 are determined by evaluating the expression (7) for the particular species of ion expected.

3.2 Electron collecting probe

For the electrons, their thermal velocity is much greater than their drift velocity, so we can use the theory for a Langmuir probe immersed in a plasma at rest which gives the current to the probe as

$$J(v) = 2\pi^{\frac{1}{2}} r^2 en \left(\frac{2kT_e}{m}\right)^{\frac{1}{2}} \exp \frac{v}{kT_e} \quad \ldots\ldots\ldots\ldots (8)$$

in the retarding region.

Now for a small spherical probe when the radius of the charge sheath around the probe is large compared with the probe radius Medicus (1961) shows that

$$J(v) = a + b V$$

in the accelerating region where for a Maxwellian velocity distribution

$$a = 2\pi^{\frac{1}{2}} r^2 en \left(\frac{2kT_e}{m}\right)^{\frac{1}{2}}$$

$$b = a/kT_e$$

That is, the variation of $J(v)$ for the accelerating region is linear and tangential to the variation in the retarding region.

This is illustrated in fig. 2. It can be seen that as a means of defining space potential, the current characteristic is not very suitable. However, if the first derivative is observed on a semi-logarithmic plot, it can be seen that it is possible to locate the point at which the probe and the plasma are at the same potential.

A further reason for measuring the first derivative of the current voltage relationship is that the effects of photo-electric currents are eliminated. In fact, the negative current to the probe is given fully by

$$J(v) = Je(v) - Jp - Ji(v)$$

where Je is given by equation (8)

Jp is photo-electric current

Ji is positive ion current

Now, Ji $\ll$ Je (see section 5) and J_p is constant.

$$\therefore \quad \frac{dJ}{dV} = \frac{dJe}{dV} \quad \text{only}$$

$$= 2enr_p^2 \left(\frac{2}{km}\right)^{\frac{1}{2}} \cdot \frac{1}{T_e^{\frac{1}{2}}} \cdot \exp\left(-v/kT_e\right)$$

in the retarding region

and $$\frac{dJ}{dV} = 2enr_p^2 \left(\frac{2}{km}\right)^{\frac{1}{2}} \cdot \frac{1}{T_e^{\frac{1}{2}}}$$ in the accelerating region.

Therefore, in the retarding region a plot of log $\left(\frac{dJ}{dV}\right)$ v. V results in a straight line of slope $-\frac{1}{kT_e}$, from which the electron temperature T_e may be found, while in the accelerating region log $\left(\frac{dJ}{dV}\right)$ remains at a constant value depending on $\frac{n}{T_e^{\frac{1}{2}}}$ from which n may be determined when T_e is known.

Thus, although the electron probe is primarily for location of vehicle potential, it also gives supplementary information on electron density and temperature.

3.3 Total ion density probe

For a spherical probe moving through the ionosphere of a velocity of V_s and biased -ve with respect to the plasma, the ion current collected is largely independent of attitude and given by:

$$I_p = N^+ eAV_s$$

where

N^+ = total ion density

e = electronic charge

A = probe cross sectional area

V_s = satellite velocity

The only attitude dependence is caused by the probe passing into the wake of the spacecraft.

Changes in I_p are therefore a direct monitor of fluctuations in the ambient positive ion density N^+.

Since the emission of photo electrons from the probe surface adds to I_p the probe must be surrounded by a grid biased more negatively than the energy of the peak flux of photo-electrons from the surface. In this way the photo-emission current is reduced to a low value compared with the ion current.

4. Description of Sensors

4.1 Ion mass spectrometer and electron probe

As mentioned previously, this sensor consists of a sphere 19 cm in diameter to collect positive ions, and surrounded by spherical grid 20 cm in diameter biased negatively to prevent electrons reaching the probe surface. The stem supporting the grid is also at grid potential to avoid any high field strength areas in the immediate vicinity of the probe. Integral with the probe assembly is a pre-amplifier occupying one half of a cylindrical container mounted at the end of the grid supporting stem.

The pre-amplifier case also serves to support the electron probe on a short stem at right angles to the axis of the case, and the other half of the container is used as a preamplifier for this probe.

The detail assembly is shown in figure 4. The surface of both the large and small spheres are to be rhodium plated using plating techniques as similar as possible. This is to ensure that the contact potential between the two probes is low. Rhodium is chosen for the surface because of its durability, freedom from atmospheric corrosion and constancy of contact potential over a large plated area.

The two probes must be in close proximity so that the measurement of vehicle potential by the small probe is that applicable to the large probe,

and this is achieved by the mounting arrangement described above. The other criteria for positioning the probes is that they should be clear of the charge sheath surrounding the satellite, and also that they should have a field of view of as near 4π steradians as possible. These are achieved by mounting the probe assembly on a boom 1.2 metres long which is deployed to have its axis in the direction of the satellite coordinate system.

4.2 Total ion density probe

This probe consists of a rhodium plated sphere 9.0 cms in diameter surrounded by a spherical grid 10.0 cms in diameter. The sensor is mounted on a boom projecting from the spacecraft skin aligned with the spin axis. The assembly is shown in figure 5.

The probe is biased to a negative potential to collect positive ions and the surrounding grid to a more negative potential to supress photo-electrons emitted from the probe surface.

There are no preamplfiers associated with this probe, the only electrical components in the vicinity of the probe being those to decouple R.F. signals picked up by the probe.

5. The Problem of Spacecraft Potential

In making probe measurements one is eventually faced with making voltage biasing measurements relative to the spacecraft as a reference. However, this is not tied to a large capacity body such as the earthing used in ground-based observations, and since we need to know these potentials relative to the ionosphere, it is important that the spacecraft adopts a potential not far removed from the ionosphere, and also that it remains stable.

When a satellite is moving through the ionosphere it tends to become negatively charged due to collection of electrons and positively charged due to collection of positive ions and photo-emission. If no point on the satellite generates an electric field from an internal source of potential, the spacecraft normally stabilises its potential at about one volt negative

to the ionosphere, at which potential the electron current equals the ion current plus the photo-electric current. If, however, there are any surfaces at positive potentials, they collect electrons, and unless this electron current is neutralised by providing sufficient clean metal for an increased ion current, the satellite will charge up to a relatively high negative potential.

The ratio of the electron current when a probe is at space potential to the ion current when an area of metal is also at space potential is given by

$$\frac{Je}{Ji} = \frac{Ae}{Ai}\sqrt{\frac{m_i}{m_e}}$$

where Ae = area collecting electrons
Ai = area collecting ions
m_i = mass of ion
m_e = mass of electron.

$\frac{Je}{Ji}$ must be unity at equilibrium

$$\therefore \quad Ai = Ae\sqrt{\frac{m_i}{m_e}}$$

$$= 170\ Ae \text{ for } O^+ \text{ ions}$$

Now, if Ai is chosen to be this value the potential of the satellite will stabilise at some point about midway between zero and the maximum negative charge attained with equal ion and electron collecting areas. Furthermore, any variation of electron current collected will cause large variations in the spacecraft potential acting to counteract the sweep voltage being applied to the probe which would cause these changes in electron current.

We, therefore, make the ion collecting area

$$Ai \gg 170\ Ae$$

so that the potential stabilises quite close to zero and changes in electron current have a very small effect on the satellite potential.

Thus, for the S45 experiment we have specified a clean area of 5000 sq. cm. to compensate for the current collected by a spherical electron probe of 1 cm. in diameter.

The calculations presented above are not exact because, of course, the ratio of $^{Je}/Ji$ is for space potential surfaces, whereas a different potential is reached by the spacecraft. Accurate calculation is difficult because the current collecting characteristics of an irregular body such as the clean areas of the spacecraft is not readily predictable. However, the calculation serves to give an indication of the minimum clean area required.

6. Description of Electronics

The overall block diagram of the electronics is shown in fig. 7.

6.1 Mass spectrometer signal processing

The mass spectrometer probe has a varying sweep voltage applied to it in a manner described below, and added to this relatively slowly varying voltage are two alternating voltages at frequencies f_1 and f_2 and equal amplitudes the value of which is of the order of kTi where Ti is the mean ion temperature expected (about 1000°K), and can be commanded to a lower amplitude. Non-linearities in the probe current/voltage relationship cause mixing of the two a.c. signals, the degree of mixing depending on the second derivative of the i-v characteristic. Thus, by observing the amplitude of the current at the difference frequency $(f_1 - f_2)$ a measure of the second derivative of the probe characteristic is obtained as the sweep voltage changes.

$$J_{(f_1 - f_2)} = v_1 v_2 \frac{d^2 J_i}{dV^2}$$

where v_1 and v_2 are the amplitudes of the f_1 and f_2 signals. By filtering the current flowing to the probe the difference frequency component may be selected and rectified to obtain a measure of the value of $\frac{d2J_i}{dV^2}$. In fact, the expected dynamic range of $J_{(f_1 - f_2)}$ is about 80 db, so to obtain measurements over all conditions likely to be encountered in orbit the current is monitored by a logarithmic amplifier having four overlapping ranges. The form of the calibration curves for the amplifiers being as shown in fig. 8. During any one sweep two of the ranges only are used, either the high or low sensitivity pair, selection of the pairs being automatic and alternated from sweep to sweep of the probe voltage. A monitor of which sensitivity range is being used is kept by altering one of the experiment housekeeping channels to a preset value during one

sensitivity mode and monitoring the housekeeping signal during the other sensitivity mode.

6.2 Electron probe signal processing

The electron probe also has a sweep voltage applied to it and, in addition, a single alternating voltage f_3 of small amplitude less than or equal to kT_e where T_e is the smallest value of electron temperature expected to be encountered. The amplitude of the probe current at this frequency is, therefore, a measure of the mean value of $\frac{dJe}{dv}$ over the voltage defined by the amplitude of the a.c. signal. This component is filtered from the probe signal by using an a.c. bridge technique to prevent the applied signal reaching the input of the analysing amplifier when no probe current is flowing, and then using a selective amplifier to measure the off-balance component at f_3 when the probe is taking current.

Again, to cope with the wide dynamic range a logarithmic amplifier is used, but in this case only one range is used to cover a dynamic range of about 60 db. A further reason for using a logarithmic amplifier in this case is that the variation of $\log \frac{dJe}{dv}$ in the retarding region is a linear function of voltage as explained earlier.

6.3 Generation of sweep voltages

Previous experience in this type of probe has shown that the caution necessary to cope with unexpected variations in spacecraft potential has often led to considerable fractions of the data being transmitted when both electron and ion probes were so negative with respect to space potential that no useful information was obtained. To improve this situation a new technique has been adopted in sweeping the potential.

If we consider the start of a sweep cycle when both mass spectrometer and electron probes are at about -5 volts relative to spacecraft ground. The sweep generator produces a rapid increase in voltage on both probes until the signal from the electron probe rises above a certain threshold. At this time the sweep rate reduces to about 1 volt per second for both probes, and the electron probe changes the origin of its slowly rising region of sweep voltage. This is illustrated in fig. 9.

The effect of this is to bring the probes rapidly to about 1 volt below space potential, then to allow the mass spectrometer to increase slowly from that point, while the electron probe sweep voltage is reduced in order that

signals below the threshold may be studied.

When the ion probe voltage reaches a certain preset level both sweep voltages fly back to the starting point of about -5 volts.

It is not possible to specify an exact sweep period, the period is a function of electron temperature and spacecraft potential, but it is of the order of 10 seconds when operating in the searching mode.

Should the electron probe became faulty it is possible to change the mode of the sweep voltages to that of a normal repeating sawtooth waveform between defined voltage limits, on issuing one of the commands allocated to this experiment.

6.4 Total ion density probe signal processing

The current flowing to the total ion density consists of a relatively steady level (on a time scale of a few seconds) superimposed on which may be small fairly rapid variations caused by the spacecraft passing through irregularities in the ionosphere.

The circuitry separates these two components of the probe current in order that both the ambient ion density and small fluctuations may be observed. The mean d.c. current is amplified by a logarithmic amplifier and its output is presented to one of the low speed telemetry channels.

The fluctuating component is treated in a somewhat different manner. A circuit has been devised which gives an output to the telemetry

$$V = \frac{5}{\left(\frac{Io}{Ip}\right)^{\alpha} + 1} \quad \text{volts}$$

where Io = current to probes at beginning of mass spectrometer sweep

Ip = current measured during the course of the sweep

α = preset sensitivity constant

Now the circuit automatically sets Io = Ip at the beginning of each mass spectrometer sweep, so

V = 2.5 volts,

then, depending whether Ip increases or decreases, the output voltage varies in a manner shown in figure 10.

It is planned to set α to a value greater than 10 so that very small fluctuations in (Io/Ip) of 1% or less may be detected. The circuit will then

provide a measure of the small fluctuations which will have only a minor effect on the mass spectrometer, but are of geophysical interest; however, if a large fluctuation in ion density should occur this will be indicated by a zero or full scale reading of the output which will be an indication that the mass spectrometer data is suspect.

6.5 Electronics housing

Most of the electronics described is housed in a single electronics box located in the experimental area of the satellite. In addition, there is an AC/DC convertor to provide the voltage rails for the electronics from the spacecraft AC power supply. The whole unit weighs 1.9 Kg and consumes 400mW of electrical power.

The only electronics separate from this unit are two preamplifiers housed in a case on the boom containing the mass spectrometer.

6.6 Telemetry channels

The experiment uses 15 telemetry channels of which four are sampled at 0.15 sec intervals, two at 1.2 sec intervals and nine at 4.8 sec intervals. The quantities being measured are shown in fig. 7 and tabulated in Table I.

6.7 Command facilities

There are six commands used by the experiment to change sweep mode, bias voltages and a.c. amplitudes. These are tabulated in Table II.

7. Laboratory Stimulation of Probes

7.1 Mass spectrometer and electron probes

The current voltage characteristic of a diode is similar to that of a Langmuir probe in the ionosphere, and for this reason a diode with a suitable series resistance to limit the conduction current is connected to the probe. As the probe voltage is swept, the analysers then produce outputs of similar form to those expected in the ionosphere.

Precautions have to be taken in shielding the diodes to avoid unwanted signal pick-up, and also it is necessary to use a series combination of a point contact diode and a junction diode to give both low capacitance and low leakage current. In the case of the mass spectrometer two diodes will be used and by applying different bias voltages the situation of two ion species can be simulated.

The diode stimulation for both the mass spectrometer and electron probes will be housed in a shielded container mounted on the boom assembly with connections taken to the probe through contacts specially provided on the two probes.

7.2 Total ion density probe

In order to stimulate the steady current to the total ion density probe it is only necessary to connect a resistor between the probe and spacecraft ground. The fluctuating component of the ion current will be simulated by a low frequency oscillator powered by the voltage on the guard ring of the probe assembly.

The components to achieve this will be mounted on the protective covering of the probe surfaces which will have contacts on to the probes in addition to providing protection.

References

1. Mott Smith, H.M. and Langmuir, I. 1926, Phys. Rev. 28, 727.
2. Druyvesteyn, M.J. 1930, Z. Phys. 64,-790.
3. Medicus, G. 1961, J. Appl. Phys. 32, 2512.
4. Medicus, G. 1962, J. Appl. Phys. 33, 3094.
5. Norman, K. and Willmore, A.P. 1965, Planet. & Spa. Sci. 13, 1.

TABLE I

Telemetry channel	Sample Interval (sec)	Measured parameter
1	~~0.15~~ 0.2	Ion probe 2nd derivative (high sensitivity)
2	~~0.15~~ 0.2	Ion probe 2nd derivative (low sensitivity)
3	~~0.15~~ 0.2	Electron probe 1st derivative
4	~~0.15~~ 0.2	Plate probe fluctuations
5	1.20	Ion probe sweep monitor
6	1.20	Electron probe sweep monitor
7	4.80	Total ion ~~Plate~~ probe mean current
8	4.80	a.c. amplitude monitor (f_1)
9	4.80	a.c. amplitude monitor (f_2)
10	4.80	a.c. amplitude monitor (f_3)
11	4.80	d.c. supply monitor A
12	4.80	d.c. supply monitor B
13	4.80	main package temperature
14	4.80	bias monitor
15	4.80	preamplifier package temperature

TABLE II

Command	Function
1	a.c. level, sweep, bias all mode 1
2	a.c. level 2
3	sweep mode 2
4	bias level 2

List of figures

SPHERICAL ION PROBE - 2nd DERIVATIVE FUNCTION

IONOSPHERIC DRIFT VELOCITY = 7.75km/sec

COMPOSITION $H^+ = 0.01$

$H_e^+ = 0.24$

$O^+ = 0.75$

TEMPERATURE 500°K

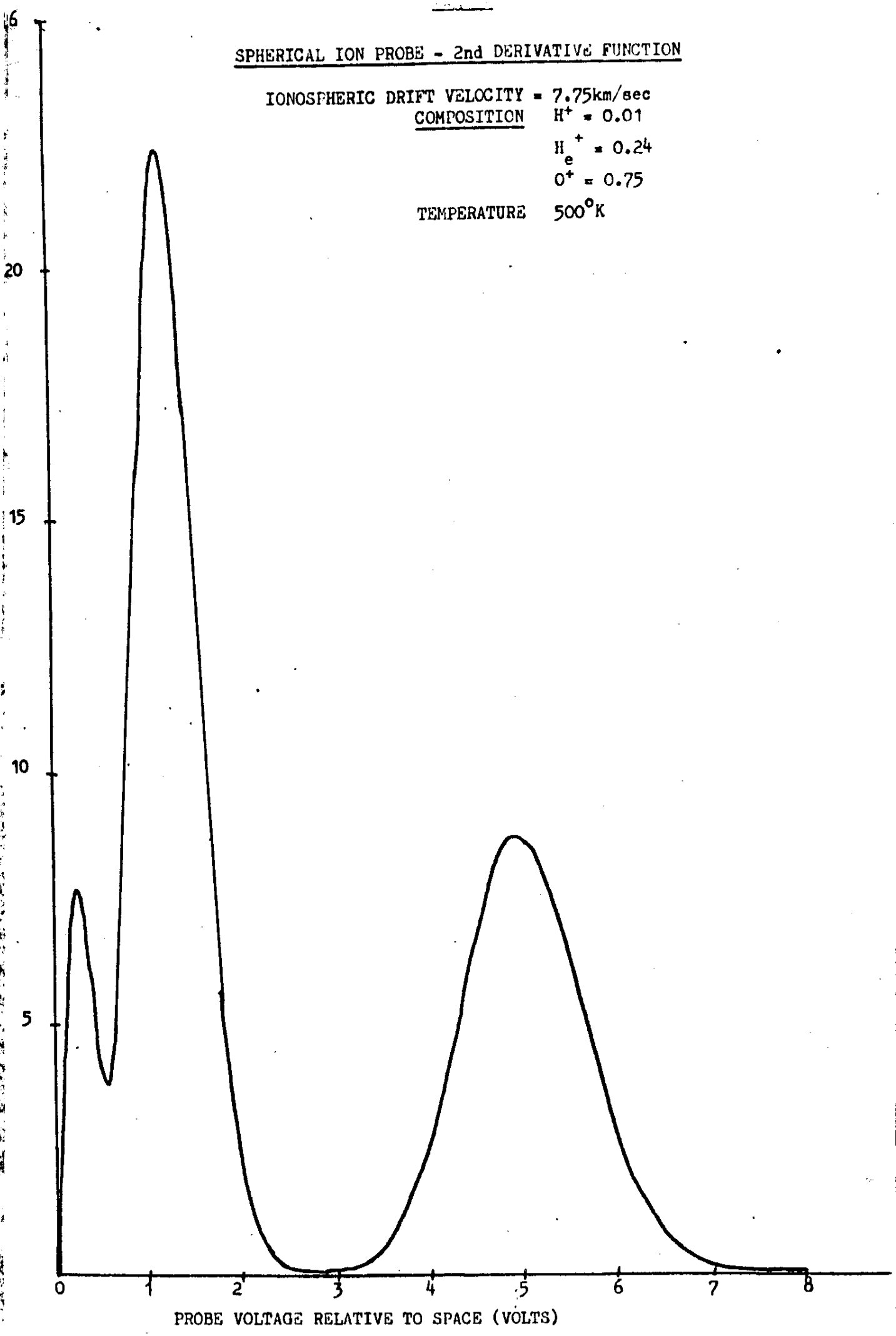

Fig. 2

Variation of electron probe current and its first derivative

$T_e = 1500^{\circ}K$

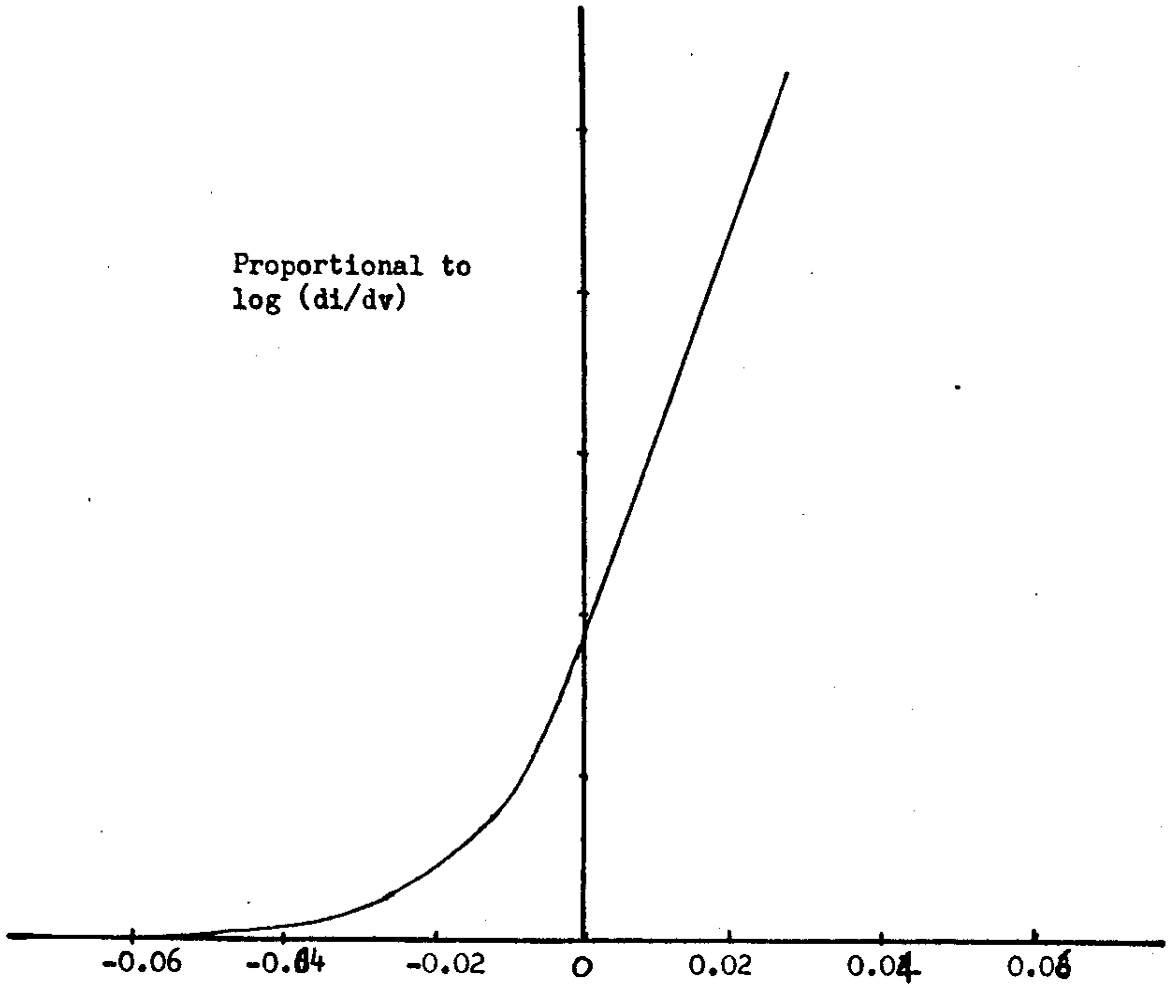

Fig. 6

Form of Ion Probe calibration curves

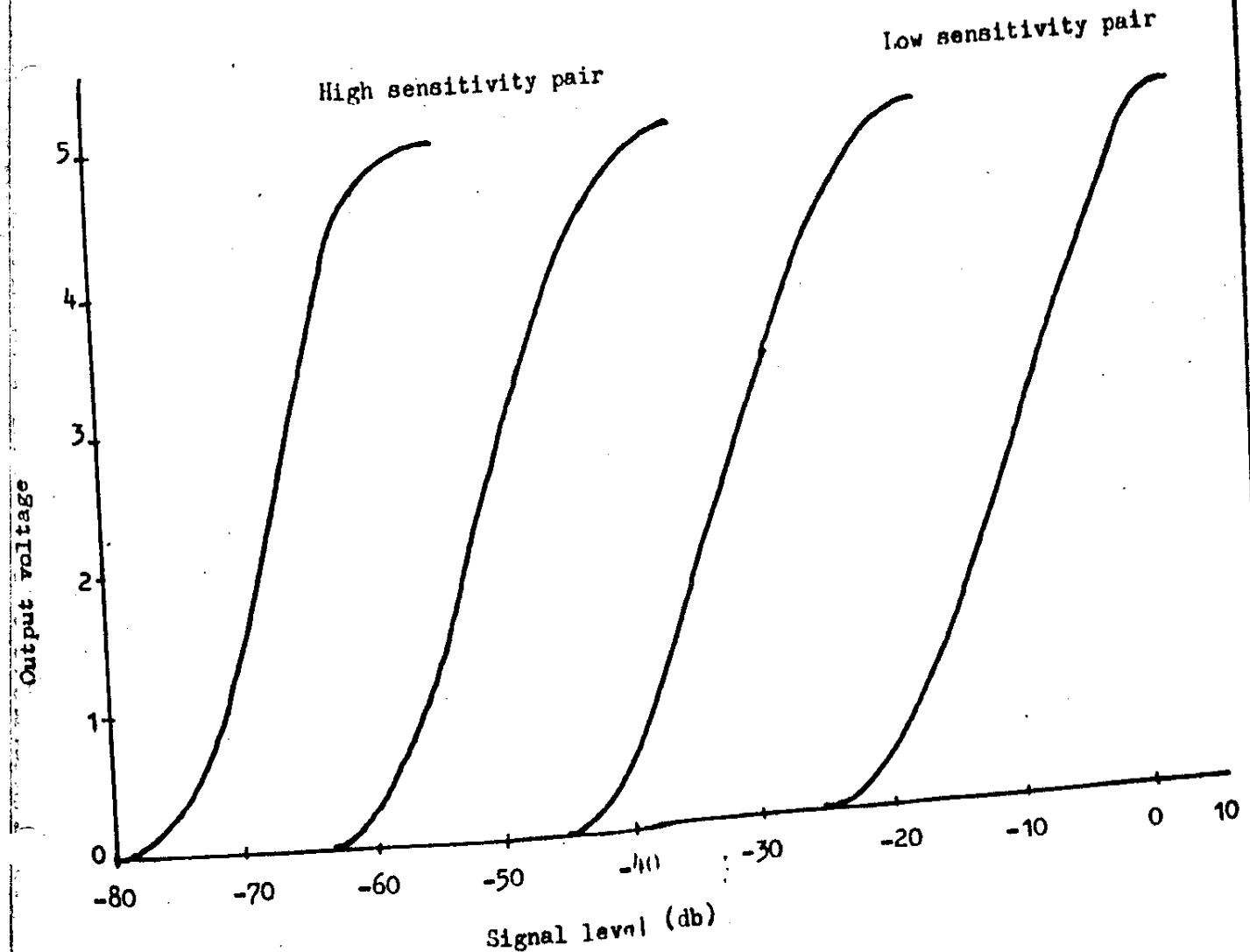

Ion and electron probe sweep waveforms

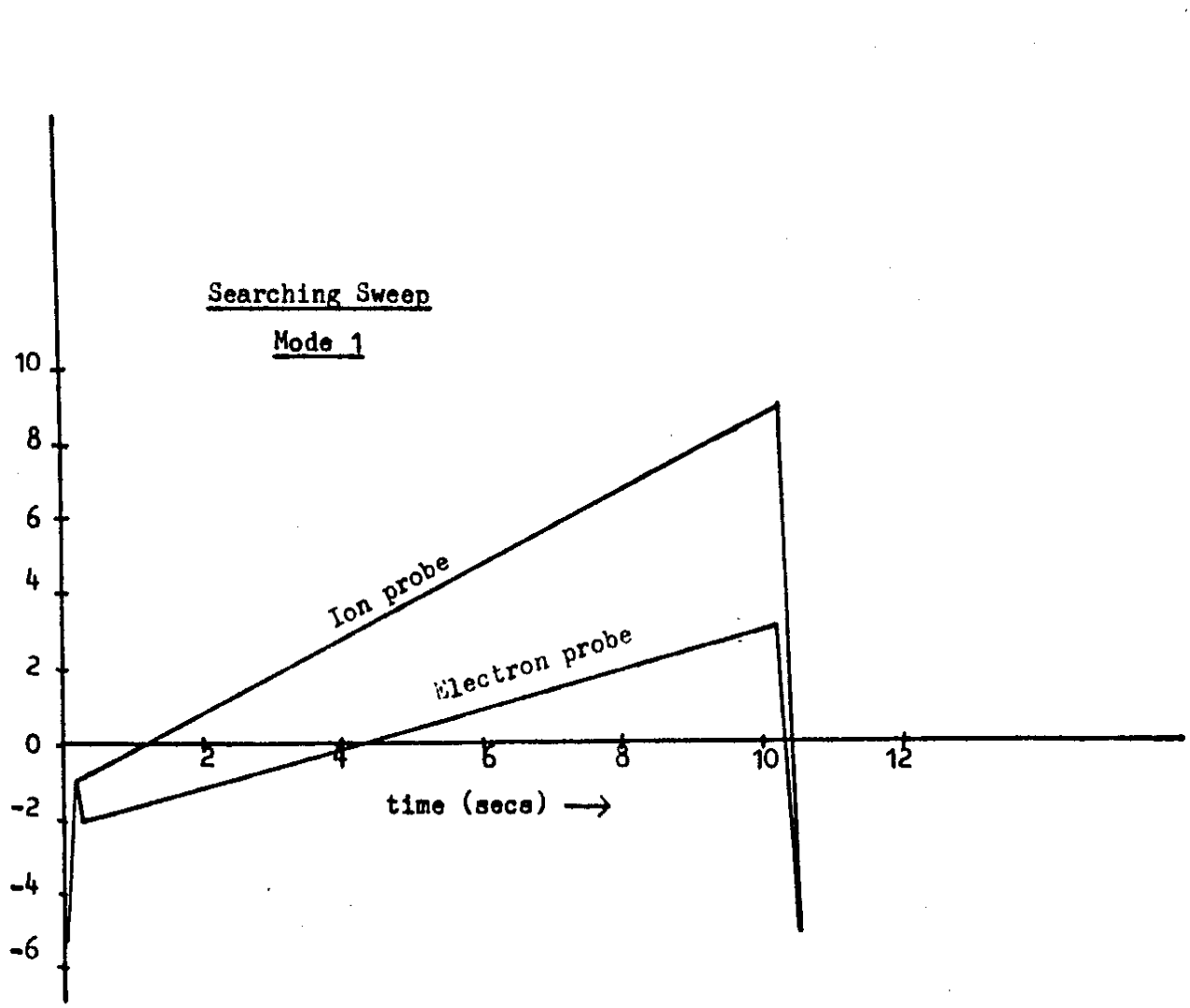

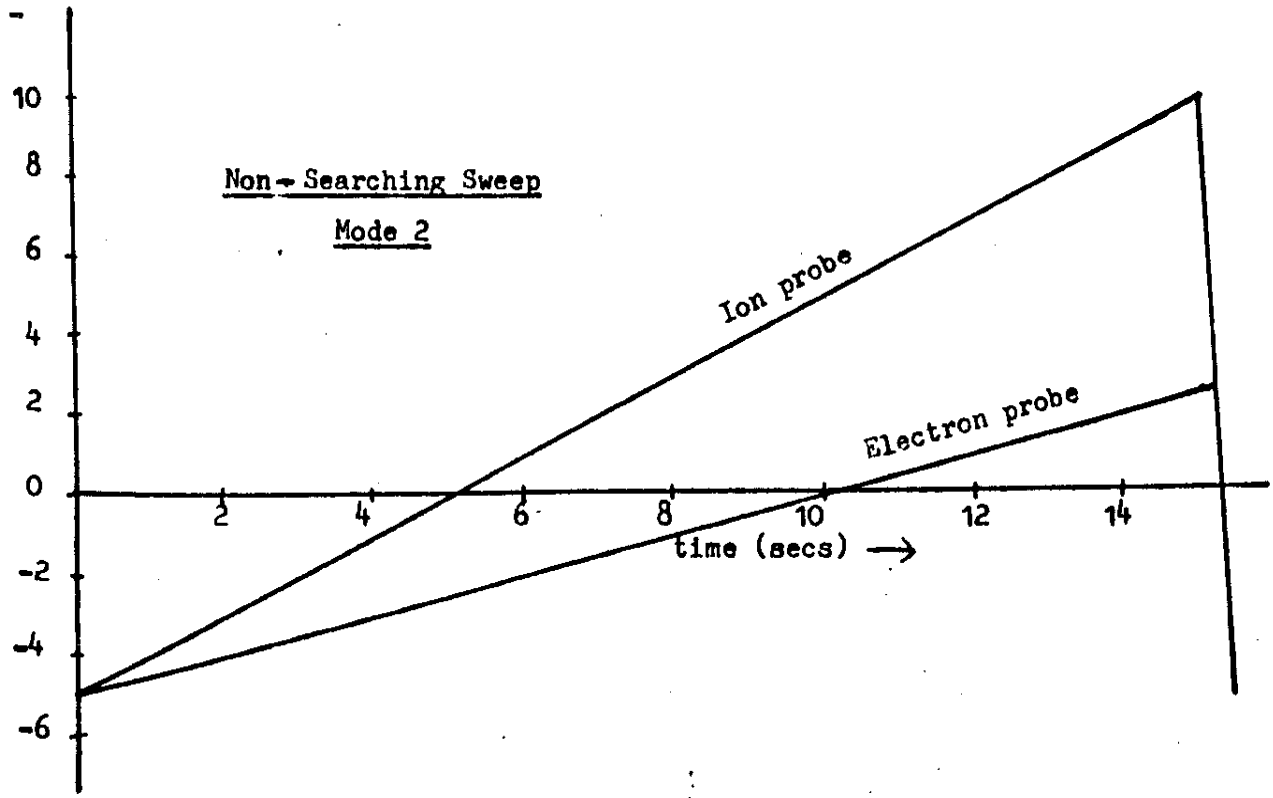

Fig. 8

Transfer characteristic of circuit for monitoring
Small fluctuations in plate probe current

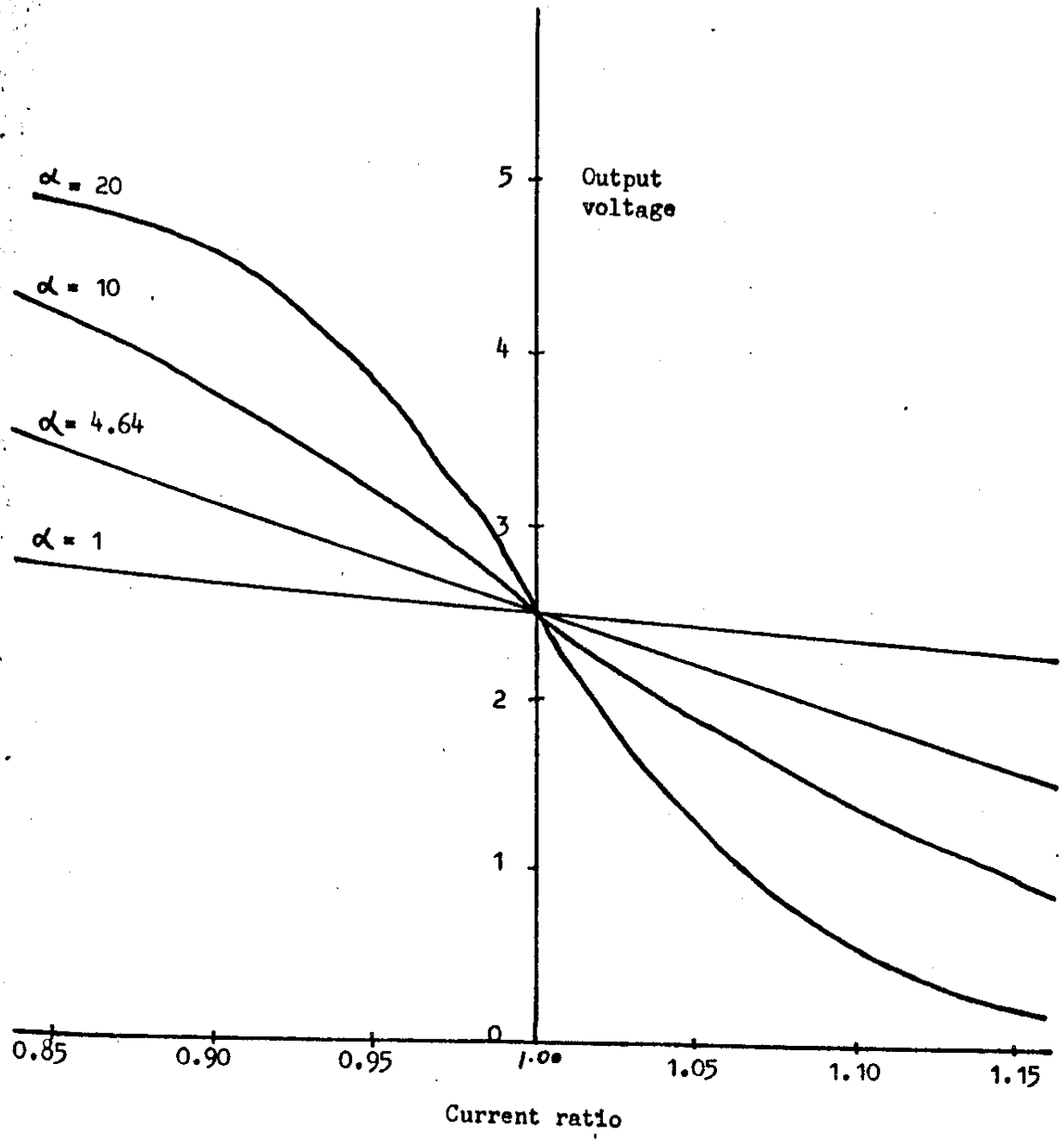

72-092A-01

ESRO-4 - EXPERIMENT S45

POST LAUNCH REPORT

W.J. Raitt

Mullard Space Science Lab.

24th August 1973

Summary

The report describes the form of the S45 raw data and the format of the data tapes received from ESOC. The procedures to handle this data both from a routine administrative point of view and the reduction to geophysical parameters is described. A preliminary description of the type of results obtained at this early stage is given together with an outline of the larger scale scientific analysis which could commence in the near future.

Table of Contents

ESRO-4 EXPERIMENT S45

POST LAUNCH REPORT

AUGUST 1973

1. Introduction

The satellite ESRO-4 was launched at 00.17 U.T. on 22nd November 1972 from the Western Test Range at Vandenberg Air Force Base, California. It successfully achieved an orbit of the earth but the apogee of 1100 km was about 100 km high and the perigee of 250 km was about 30 km low from the nominal orbit specifications. The inclination and time of launch met the scientific requirements. The nominal spin rate of about one revolution per second was achieved after boom deployment. The moment of inertia of the spinning satellite constituted the means of its stabilisation, although, as will be mentioned later the direction in which the spin axis points can be changed by commands sent from the ground.

The experiments carried by the satellite were as follows:-

Code	Institution	Objectives
1. S45	MSSL, London	Thermal plasma parameters of ionosphere
2. S80	Univ. of Bonn	Neutral mass spectra of atmosphere
3. S94	Kiruna Geophys. Obs.	Particle fluxes 0.5-150keV, electrons and protons
4. S99	Univ. of Utrecht	Proton fluxes 2-100MeV, Alpha particles 4-240MeV
5. S103	MPI, Garching	Proton fluxes 0.2-90MeV, Alpha particles 2.5-360MeV
6. HCI	Estec, Noordwijk	Assess operation of Infra red horizon detector

The satellite subsystems included a tape recorder, a high and low bit rate encoder with separate transmitters and a magno-torquer to re-orient the spin axis of the satellite.

The S45 experiment consists of three sensors and associated electronics packages designated as follows:-

Code	Function
S45/1	Spherical ion mass spectrometer (20 cms diameter)
S45/2	Spherical electron Langmuir probe (1 cm)

Code	Function
S45/3	Gridded spherical total ion current collector (10 cms)
S45/4	Main electronics package inside spacecraft
S45/5	S45/1, S45/2 preamplifier package (boom mounted)

The positions of the probes relative to the spacecraft is shown in fig 1.

The satellite was launched with S45 switched on, and as soon as the nose-cone had been ejected telemetry signals received at the range showed characteristic curves from the S45 electron probe. The other experiments were switched on in sequence during the first week of orbital operation and all were found to function satisfactorily.

There are a number of standard spin axis pointing directions which are normally such that the spin axis lies in the orbital plane of the satellite. On one occasion it was 30° out of plane to improve the collection of energy by the solar cells. A list of the standard attitude and the transition dates is given in Appendix I.

Further information on the facilities of the satellite and the operational programme can be obtained from the ESTEC documents:-

E4/PD/06	Issue 3	Mission and Operational Programme
E4/PD/10	Issue 3	General Description of the ESRO-4 Satellite

2. General Characteristics of the Data

The general form of the received data will be made with reference to copies of Sanborn chart records made at ESOC and supplied on a routine basis to enable rapid assessment of the operation of the experiment on a quick-look basis.

2.1 S45/1 Data

The peak in the second derivative of the probe current-voltage characteristic as ions of differing mass are retarded is shown in fig 2. These plots show the automatic change in operations range occurring at each fly-back and flagged in one of the housekeeping data samples.

The rapid motion of the satellite through the earth's magnetic field causes a voltage to be induced in the boom given by

$$V_{ind} = (v \times B) \cdot L$$

where v = satellite velocity vector
B = magnetic field vector
L = boom vector

} all in same coordinate system

During one sweep v and B remain sensibly constant, however L is a rotating vector at the spin rate of 1 revolution per second. Thus the induced voltage is oscillatory and, being added to the probe sweep voltage, it causes a modulation in the signal received by the probe current analyser.

The induced voltage disappears at the magnetic equator when v and B are virtually parallel and is maximum at the polar regions when v and B are perpendicular. The effect of this on the S45/1 data is shown in fig 3.

The general noise level shows similar characteristics to the ESRO-I results, in the regions of the characteristic when the second derivative should be very small the output signal shows a higher noise level before the ions are retarded, that is if i is large there is a larger 2 kHz component than if i is small after the ions have been retarded. The latter level has changed negligibly since the pre-launch measurements, a contrast to ESRO-I when the residual electronics noise level steadily increased over the first 6 months in orbit.

A feature of the ESRO-I data which has not been observed in ESRO-4 is the large increase in noise level such as to swamp the characteristic peaks which occurred when ESRO-I left the polar regions and progressed towards the equator. It may be that sufficient orbits in the right sort of altitude/local time conditions have not yet been studied, however my feeling at present is that if the effect is there at all it is at a much lower level than was observed on ESRO-I.

There is a small amount of RFI observed when the high power transmitter is operating, this is a surprising result since the last three RFI checks on the ground showed no interference at all. The form of this interference is shown in fig 4. The high power transmitter is used most during attitudes favourable to the S94 experiment and then only over the northern auroral and polar cap regions. It is also used for tape recorder dumps which last about three minutes.

In general the S45/1 data is free from disturbance due to the satellite wake, however in certain attitudes the boom passes through the wake of the satellite and when this occurs in equatorial regions a drop in signal once per spin can be seen in the ion peaks. An example of the effect on the O^+ ion peak is shown in fig 5. This data is potentially very interesting for wake-effect studies since with careful analysis a comparison between H^+/He^+ depletions and O^+ depletions could be made. The amount of data on the ion density in satellite wakes is very sparse so it would seem worthwhile to try

and produce not only ion-wake measurements, but also profiles for different ion species.

2.2 S45/2 Data

The S45/2 probe has its first derivative measured and the typical forms of the characteristics are shown in fig 6. Again this probe suffers from the induced v x B voltage on the boom causing a pronounced spin modulation of the data.

The sensitivity of this probe was set rather high so that useful measurements could be obtained down to considerably lower densities than on earlier flights of the sensor. Also since in one mode of operation of the experiment it controlled the sweep generator it was felt that we should maintain the sweeping potentials to the probes for as much of the orbit as possible.

The result of this as far as the data is concerned is that at low latitudes near perigee during the day the probe current analyser saturates and there is no electron density measurement, however we can still measure electron temperature, and the vehicle potential measurement is not in error by more than about 200-300 mV. This latter figure could be corrected by use of the measured electron temperature and the ion density measured by S45/1.

The sweep generator stops when the instrument is operated in the scanning mode when the value of Ne falls below a value in the range 200 to 500 cm^{-3} depending on the prevailing electron temperature.

2.3 S45/3 Data

The direct ion current flowing to this fixed bias sensor is analysed in two ways on board the satellite. At every flyback the current is sampled and telemetered at relatively infrequent intervals (about 3 times during a sweep). At the instant of sampling a channel with a much faster sampling rate is set to midscale and it then monitors changes in the ion current from the sampled value with a full scale range of about $\pm$ 30%. Thus it is possible to study quite fine detail in ion density structure over a wide dynamic range.

The steady current shows orbital variations which reflect the change in ion density with altitude and latitude which will be referred to later. The profiles obtained are, however, greatly modified by the passage of the probe through the wake of the satellite which occurs once per orbit at a relatively slow speed since the probe is on the spin axis, and the spin axis is in the orbital plane.

The fluctuations in ion current have three typical types of signal shown

in fig 7. Fig 7a is typical of an undisturbed region and the general variation over the sweep is probably a combination of altitude and latitude variations of density occurring during the sweep period. The small residual spin modulation is thought to be due to transparency fluctuations in the grid surrounding the probe. When the probe is over the auroral and polar regions the data shows large and random variations indicating either temporal or spatial fluctuations in ion density due to incoming charged particles. A typical section of this data is shown in fig 7b. Another characteristic form of the data is shown in fig 7c which was taken as the S45/3 probe was entering the wake of the satellite. The large ion density gradient in this region will cause severe modulation of the ion current if the probe is slightly off the spin axis causing it to effectively oscillate in the region of high density gradient at the spin rate. During static ground deployment tests the alignment of the probe to the spin axis was always estimated to be better than 1 degree, thus if this figure can be relied upon in orbit it would enable a measurement of the density gradient in the flanks of the ion wake to be made.

3. Modifications of Experiment Mode of Operation by Telecommand

There are three parameters of the experiment which can be altered by telecommand to one of two states and any combination can be set up by sending a particular grouping of the four commands available to the S45 experiment. The commandable functions are:-

	Normal	Alternate
1. S45/1 ac voltages	200 mV	50 mV
2. Sweep mode	Fixed period and voltage range	Controlled by S45/2 signal
3. S45/1 & S45/3 Bias	-6 volts	-10 volts

The satellite was launched with everything in normal mode, then during the early orbit phase each of the three alternate modes was tested for one complete orbit on two successive days.

The behaviour of the instrument was as expected and after assessment of the data it was decided to operate the instrument with the S45/1 ac voltages at 200 mV, the sweep mode in the alternate condition and the S45/1 grid and S45/3 bias at -6 volts.

The ac voltage control is rather historic than useful since at the time of proposal for TD2 we were concerned about the effect of finite ac voltage on the shape of the light ion peaks, however since then we feel that a complete Fourier analysis of the probe signal can completely take care of the distorting effect of the ac voltage. Thus it is better to use the 200 mV level to obtain the best sensitivity for the probe.

The alternate sweep mode enables the period of the sweep generator to be changed from about 18 secs to 12 secs so improving the spatial resolution of the measurements. This mode does cause the sweep generator to stop when the electron density falls below about 500 cm^{-3}, however by this time the S45/1 and S45/3 probes are giving no data.

The control of the grid bias was put on to see what effect this bias had on the operation of the S45/1 mass spectrometer. The initial experiments and subsequent experiments have shown that this has no measurable effect on the peak being observed and furthermore it demonstrates that the S45/2 probe is sufficiently far from the S45/1 grid not to be influenced by its potential. This is shown in fig 8 which is quite a convincing demonstration of the Debye shielding effect in a plasma.

The only other commanding activity has been to revert to normal sweep mode for occasional orbits to enable a check to be made on the residual noise level of S45/2 which is otherwise not monitored when operating in the alternate sweep mode.

4. General Survey of Data Processing Procedures

The agreed procedure for distribution of ESRO-4 data to the experimenters was that each experimenter would receive magnetic tapes containing his own data and any other relevant measurements stripped from the telemetry encoder format merged with various orbital and attitude measurements and flagged with the Universal Time of the observations. The principle was adopted that in general orbit, attitude and associated parameters such as the magnetic field would be given in terms of basic vectors in a unified coordinate system, namely Geocentric Equatorial Inertial (GEI). The subroutines to manipulate these vectors into the more usual coordinates were supplied by ESOC.

Experimenters had the option of having their data in binary or BCD format on the magnetic tapes. Since the tapes were being produced on an IBM 360 computer we would have no difficulty in handling the data in internal binary form so we decided to use this tape format with its advantages in reduction of total tape volume and speed of input to data processing programmes.

The content and format of the tapes are given in Appendix II copied from information supplied by ESOC.

The only data medium we initially received was magnetic tape, so the first priority was to produce indexing and listing programmes to present the data in an easily readable form with the position coordinates reduced to conventional parameters. Also the calibration tables produced from the calibration measurements made by Pye Ltd. were used to enable the printouts to be produced in engineering units. These programmes exist to produce listings both on the line printer and on microfilm for use in the routine processing to be described later.

At the same time routines were developed to analyse the data to produce geophysical parameters from the raw data and these routines have been incorporated in a variety of programmes to make individual analyses of specific time periods from the accumulating store of data tapes. The general methods employed will be described later in sections 5 and 6.

Once sufficient data had been analysed to gain confidence in the automatic analysis procedures adopted the various routines were incorporated into the main data reduction programme which analyses complete or part data tapes and builds up a master tape of the reduced geophysical parameters. Details of this programme will be given in section 6.

Having referred to the various categories of programme, the general procedures adopted in handling the data can now be outlined.

The tapes arrive by post from ESOC and are logged into a tape receipt form. The tape is then labelled Qxxxxx and a blank tape labelled Bxxxxx where xxxxx is the ESOC tape number. At the next available opportunity the tapes, together with an equal number of blank tapes, are sent to the UCL Computer Centre to be stored in tape racks which have previously been vacated by shipping tapes not immediately needed back to the tape store at Flaxman Terrace. There is no paperwork with the ESOC tapes so the first job is to index the tape to find how many files are written on it, this being done the Q-tape is then copied to the B-tape using a UCLCC programme which makes a "carbon copy" of the original tape. When the copy has been made the Q-tapes are then stored at Flaxman Terrace and the B-tapes at UCL as far as is possible within the limited tape storage space available at UCL.

The tape indexes are then used to select files which enable routine listing programmes to be run in which a few sweeps are listed once per day and about two thirds of an orbit once per week. The latter printout is produced on micro-

film using the SD 4020 plotter situated at the Atlas Computer Laboratory, Chilton. These printouts are archived for reference purposes. Each tape is also run with a programme which produces a chronological file of all available data. This file is stored on disc and can optionally be listed from time to time to produce an index of where data for specific time can be located on the original data tapes.

Within the last month we have begun running the main production programme to build up the master data tapes. Since it is planned to reduce all data by this programme we are analysing the data tape by tape in numerical order of ESOC tape numbers, in fact it turns out that this is approximately in chronological data order. This is proving to be quite a time consuming process because of the large amount of data available. Each tape recorder playback of one orbit's worth of data takes about 1.5 minutes of computer time to process and we are nearly up to orbit 4000 with 80-85% data recovery. It is hoped that operations can be transferred to the RHEL computer which should improve the time by a factor of 4-5 since the programme is compute-bound rather than I/O-bound.

At present this phase of the processing is proceeding rather slowly because we cannot get about 1 hour per night every night due to the unusually high work-load at UCL this summer. However, we have managed to make a good start on the processing by making use of a whole shift on two Sundays recently.

A list of all data processing programmes produced to date is included in Appendix III.

5. Problem Areas

In general there have not been many purely data processing problems, the tape reading procedures have been quite straightforward, thanks largely to a very useful routine MULTIR developed by the UCLCC for handling multi-file tapes which is otherwise rather cumbersome on the IBM 360. The greatest difficulties in analysing the data have arisen from the radial boom-mounted position we had to accept and from a basic limitation of the S45/1 probe in analysing the light H^+/He^+ ions.

5.1 Spin modulation corrections

The cause and effect of spin modulation in the S45/1 and S45/2 data has been described earlier in section 2.1. Sufficient attitude information is supplied with the data such that, in conjunction with the spin phase monitor data, it is possible to compute the induced voltage ($v \times B$). L at any sample time of the S45/1 or S45/2 data in order that the monitored probe voltage

can be corrected. The mathematical method to make this correction has been developed by J. Sojka and is described in Appendix IV. The amplitude of the oscillating voltage was calculated satisfactorily, but the phase gave us the greatest difficulty. It proved impossible to get the best cancellation of the spin effects using the nominal boom position and data time reference, so it was necessary to introduce a variable phase offset and inspect the data plots to see which was the best phase offset from nominal to use. It appeared that this figure should be about 12^{o} phase offset. Examples of the spin modulation correction to the S45/2 data is shown in fig 9.

When the spin voltage correction is applied to the S45/1 data the removal of the modulation is not so effective as is shown in fig 10. One possible cause of this is due to the overall time constant of the S45/1 circuit from probe to telemetry output which would cause an additional phase lag in the signal. This parameter was deliberately reduced during the circuit development in anticipation of this problem. However, noise considerations prevented Pye from reducing the time constant below about 50 m sec. This figure is still small compared with the interval between samples of 200 m sec and the spin period of 500 m sec so I think we are still talking of a relatively small correction.

The response of each of the four operating ranges of the instrument was measured on the bench and it is hoped that the effect of this correction on the S45/1 data can be studied in the near future if the manpower to do so is available.

The procedure outlined above is only applicable when the satellite is in sunlight. In darkness there is no spin phase measurement available from the sun sensor and in this case we resort to our own data to obtain the spin induced voltage oscillation. As explained in section 6.2 the oscillating probe voltage component can be derived from a function fit to the retarding region of the S45/2 output, then providing the data and hence the fit is good this function can be used to correct the probe voltage monitored for the S45/1 probe. The transition from sun to dark and vice-versa is automatically detected by analysing the spin phase output and the method of correcting the S45/1 voltage automatically selected in the programme.

5.2 Analysis of Light Ions

This is a problem which has really been carried over from the ESRO-I data analysis. The basic problem is the low mass resolution of the instrument causing the H^{+} and He^{+} peaks to overlap thus making peak width measurements a

function of both H^+/He^+ ratio and ion temperature. A relatively fast method of reducing this data was developed to a certain stage for the ESRO-I data and has been described in a recent paper in the Journal of Physics E: Scientific Instruments (Raitt et al, A satellite-borne positive ion mass spectrometer, 6, 443, 1973). However, it has not yet been possible to refine this procedure to the stage at which it can be incorporated into routine processing. I think again it is time and effort which is required rather than a basic difficulty, and I am hopeful that J. Sojka who started to look into the analysis method will be able to return to it when the pressure of round development, testing and launching has eased after the High Latitude Campaign.

6. Procedures to Reduce Data to Geophysical Parameters

The basic subdivision of the data for all three probes are the sweeps of voltage applied to the S45/1 and S45/2 probes which are synchronized but are of different voltage range. All of the data reduction programmes therefore use the basic structure outlined by the flow diagram shown in fig 11. The box labelled "Process one sweep of data" can then represent procedures of varying complexity to analyse some or all of the probe data. The skeleton show is the logic to select all of the probe data relevant to one sweep bearing in mind the data is blocked on the magnetic tape in an asynchronous manner relative to the sweep generator which itself is not of constant repetition rate due to the control of the generator by the S45/2 signal.

6.1 S45/1 Data to Ion temperature, density and composition

After calibration and probe voltage correction for spin induced voltage peaks in the data are searched for in the two voltage ranges $Vp > 4.0$ volts, $Vp \leq 4.0$ volts, it having been found that the spacecraft potential is stable enough for this voltage to be used as a divider between the H^+/He^+ peaks at lower voltages and the O^+ peaks at higher voltages.

As far as the H^+/He^+ peak is concerned only the amplitude and position of the peak is monitored. This is sufficient to determine whether the major light ion is mainly H^+ or mainly He^+ and by using a typical ion temperature it is possible to deduce a representative ion density.

If an O^+ peak above a certain cut-off level is detected, first its amplitude and the voltage at which the peak occurs is recorded, then an attempt is made to measure its width and /or half-width to obtain a measurement of the ion temperature and density by a double interpolation in tables of theoretical widths and amplitudes of O^+ peaks as described in the paper referred to in section 5.2.

6.2 S45/2 Data to Electron Density, Electron Temperature and Vehicle Potential

The calibrated sweep's worth of data is put through a selection procedure to obtain data from the retarding region of the probe characteristic, that is the ascending section of the probe signal as shown, for example, in fig 9. A simple selection between two levels offset from the signal levels at the beginning and end of the sweep is first used, then if either too few or too many points are selected various modifications are made to endeavour to get a number of selected points between 5 and 25 in number. Should this prove impossible the temperature measurement is abandoned, Te is set to a flag value of 600 and the upper level of the signal at the end of the sweep is used to give a density value computed as if the value of Te was 6400°K.

If, however, sufficient points are selected a function of the form

$$E = A + B\,Vp + C\sin\omega t + D\cos\omega t$$

is fitted to the retarding region where

E	is the log of di/dV expressed in db
B	is the slope of the characteristic in db/volt
C and D	are related to the amplitude of the spin induced voltage
ω	is the satellite spin rate

Details of the deduction of the parameters listed in the sub-heading from the coefficients of this fitted function are given in Appendix V.

6.3 S45/3 Data to ion density fluctuation figures

It can be seen from fig 7 that in many circumstances it is difficult to define a key parameter to specify the behaviour of the fluctuations measured by this probe. However, it was decided that the data could best be fitted by a spin modulated straight line during one sweep period and this is done giving a mean slope and the amplitude of the spin component. Away from the polar regions the mean slope can be combined with the change in attitude during the sweep period to deduce a value for the scale height assuming that the change in probe current from start to end of the sweep is due solely to the change in satellite attitude. However this only gives reasonable figures over small parts of the orbit, in the majority of the lower latitude regions the latitudinal change appears to be as great as or greater than the altitude effect giving unreasonably high or low values for scale height depending whether the two effects are working together or not.

The spin rate modulation is a useful parameter since it characterises the approach to the satellite wake where it becomes very much enhanced in value as described previously.

The final parameter of the fit is the rms deviation and without looking for specific event effects in the polar region, the sudden onset of structure in the ionosphere is shown by a marked increase in the rms deviation of the fit of the function.

Preliminary data for this probe and the other probes will be presented and discussed in more detail in section 7.

6.4 The Geophysical Data Master Tape

As mentioned earlier in section 4 the parameters computed are written onto a master tape together with position, attitude and other data. The format, content and method of reading the master tape is described in Appendix VI.

7. Scientific Results Obtained

At present no large scale scientific analysis has been made due to most of the available effort being put into getting the data reduction programmes running reliably. However, as a by-product of checking the reduction programmes a certain amount of scientific analysis of the data has been made.

7.1 S45/2 Measurements of Electron Temperature, Electron Density and Spacecraft Potential

Three parameters are extracted from the measurements of the S45/2 electron temperature probe, electron temperature (Te), electron density (Ne) and spacecraft potential (Vsp).

Electron temperature . In general this is the most accurately determined parameter, once corrections for spin modulation have been made. Our analysis programme lists Te for each voltage sweep. Figure 12 shows the variations of electron temperature around a typical orbit.

Spacecraft Potential Spacecraft potential Vsp is determined by finding the voltage at which the exponential portion of the characteristic changes to a constant slope, or, in terms of the first differential which is the parameter that is telemetered, the voltage at which the idealised fixed slope of the retarding portion intersects the idealised constant level of the non-retarding portion. In practice the fixed slope has to be synthesized from the spin-modulated data, and the constant level has to be selected from a level which falls from a maximum value, and not always at the same rate. Because of these uncertainties in slope and constant level, Vsp is uncertain too, and we have to be alert to the possibility that any variations in Vsp that we may detect are in some way creations of the analysis routine rather than real effects. We expect to begin quite soon to extract Vsp from the S45/1 data, so as to have a separate and hopefully independent measurement of Vsp against which

to check the S45/2 measurements.

Meanwhile we are continuing to study the Spacecraft potential measurements, such as the example given in Figure 12, where both Vsp and Te are plotted against latitude; apogee, perigee, dark period and attitude relative to the velocity vector are all indicated. Broadly speaking Vsp follows Te as would be expected from Whipple's expression

$$Vsp = \frac{k\,Te}{e}\, m \left(\frac{T+}{Te} \cdot \frac{m_e}{m_+} \right)^{-\frac{1}{2}}$$

$$\simeq \text{constant} \cdot \frac{k\,Te}{e}$$

but there are significant departures in detail.

For the case when O^+ dominates, we can write

$$Vsp \simeq 4.5 \times 10^{-4} \cdot Te$$

but we find that, around any orbit, the constant in this expression may change by as much as an order of magnitude, from say 0.5×10^{-4} to 5×10^{-4}. In order to find out more about this variation we are listing as part of our routine analysis the ratio Vsp/Te and will look for possible correlations with other parameters.

One feature already noticed, and one which appears particularly well in Figure 12, is the dip in Vsp which occurs at or near to the equator crossings. So far we have established no rules for the occurrence and we have to be careful to disentangle it from other related effects such as changes in Te, and Ne and also changes in the position of perigee, apogee, the daylight/dark periods and spacecraft attitude. The position of the dip appears to move in relation to the equator but just what governs the movement is not yet clear; geomagnetic control so far seems unlikely.

Electron Density The electron density is calculated from a measurement of the slope of the current-voltage characteristic at space potential, and hence relies on the location of this latter parameter. Because of the lack of precision, Ne is not obtained with any very good accuracy. We are however able to compare values with the nO^+ ion concentrations given by the S45/1 probe, at least to the extent of requiring that Ne be no smaller than nO^+. Such checks have lead to the discovery that, for any reasonable criterion for determining space potential, the values of Ne during any one orbit are sometimes less than nO^+, sometimes the same and sometimes greater. As part of our current investigations we are listing the ratio nO^+/Ne in order to look for consistent trends

and for correlations with other parameters, with the hope that we may in time throw some light on this puzzling inconsistency.

7.2 Calibrations against radar incoherent scatter measurements

We have made comparisons between our determinations of Ne and Te (and nO^+) with those made by RRE Malvern using the incoherent scatter technique, on four dates in December and January last. On three of these occasions our Te and nO^+ measurements agreed well with theirs, but on the fourth a x2 discrepancy in density occurred. As far as we can tell it was due to the existence of a mid-latitude trough with its Southern edge lying in a roughly SW/NE direction, in such a position as to put Malvern outside the trough but the spacecraft inside it when crossing the Malvern latitude only 3° to the west in longitude. Taylor at Malvern has questioned the likelihood of the trough being so far south when the Kp index was fairly low, so we are checking adjacent orbits to verify its presence. A complicating factor was the occurence of dawn at the magnetic conjugate point just before the RRE measurements began. This produced a steady decay in Ne over a period of $1\frac{1}{2}$ hours or so which can, if one isn't alerted to its existence, give the impression that the trough was moving slowly southwards.

7.3 Wake Effect Observed by S45/3 probe.

The S45/3 probe passes through the wake of the satellite once per orbit at a distance of about one equivalent satellite radius. The geographic position of this passage through the wake depends to which of the standard attitudes the satellite is set, thus in attitudes 5. and 6. the wake passage occurs over one of the poles, while in attitudes 3. and 4. it occurs over the equator.

Figure 13 shows two examples of the wake as observed by this probe in which the current to S45/3 is plotted against angle of attack, and since the probe is in the -Z direction in the satellite coordinate system the maximum wake effect occurs at 0° angle of attack. The angle is given a sign to distinguish entry of the probe into the wake when θ is decreasing (180° to 0°) from the exit case when θ is increasing (0° to -180°). Figure 13a is a plot of a wake passage over the North Pole, while 13b is a plot of the wake passage over the Equator.

The two examples shown have been chosen because of the structure which appears on one side of the wake. This has been observed on a number of passes about similar times to these plots but with varying degrees of intensity.

The geometric width of the wake indicates that for parallel flow of the ions without any convergence the probe should encounter the edge of the wake

at attack angles of $\pm 42^{o}$, it can be seen that this is not what is observed indicating a convergence of the flow lines. It is not yet clear however how much this apparent convergence is affected by the negative bias on the grid of S45/3 distorting the flow as the probe approaches the wake edge.

In association with these wake profiles the fluctuations output of S45/3 shows the increased spin modulation at the edges of the wake, however as mentioned earlier in section 2.3 it is necessary to make some assumptions about the boom axis-spin axis alignment before any qualitative use can be made of the data. It is possible that this can be done by comparing the slope of the wake profile as measured by the steady current to S45/3 with the amplitude of the spin rate oscillations. A typical profile of the amplitude of these oscillations is shown in fig 14.

7.4 Location of particle precipitation zones from S45/3 data

It was described in section 2.3 that over the auroral and polar regions the characteristic appearance of S45/3 data shows large amplitude apparently random fluctuations which reveal themselves as an increase in the rms deviation of a line fitted to the data as described in section 6.3. Providing the ambient density in the altitude range in which the satellite passes over the polar cap is not too low to prevent a signal being measured the effect of the particle precipitation can be observed as shown in fig. 15.

The figure shows the orbital variation of the rms deviation during a magnetically quiet period (orbit 295) and a magnetically active period (orbit 301) about 1 day later so that the two orbits cover approximately the same geographical sub-orbital track. The main feature of both plots is the sudden increase in rms deviation at the S. Pole at the invariant latitudes marked on the diagram. The effect is rather masked at the N. Pole due to the satellite attitude causing the S45/3 probe to pass through the wake. The large amplitude spin modulations referred to earlier do seem to cause an increase in the rms deviation of the fit.

The satellite passed through its apogee of about 1100 km at the S. Pole at this time.

It can be seen that there is a significant widening of the precipitation zone when the magnetic activity is higher showing the penetration of charged particle fluxes to lower invariant latitudes, that is lower L-shells. This effect has been observed by particle experiments although there are considerable differences in the low latitude cut-off depending on particle energy, and it would be interesting to see which boundary our measured boundary agrees with most closely.

List of Appendices

Appendix I

ESRO-4 Standard Attitudes

It is easier to describe the standard attitude pictorially as shown below. The vertical line with the arrowhead towards the top of the page represents the direction of the earth's spin axis. In all cases the satellite spin axis lies in the plane of the orbit except one attitude referred to later as IA when it was set with a skew angle to bring it 30° out of the orbital plane for better collection of solar energy.

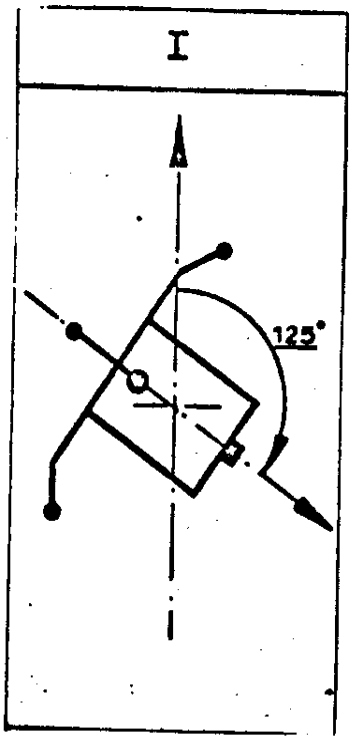

1. Designed to make satellite perpendicular to the magnetic field over Tromso for S94, also ram direction suitable for S80 when perigee near S. Pole.

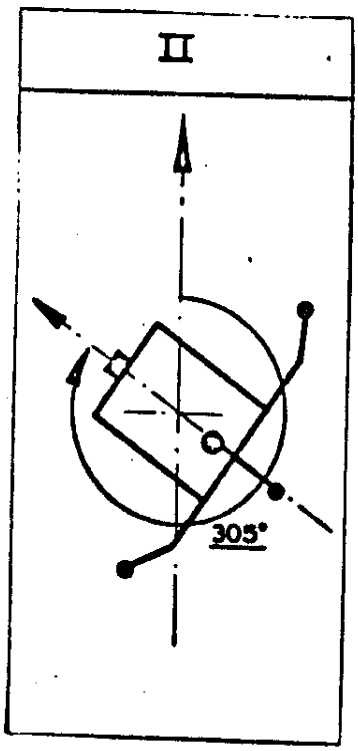

2. Designed to make satellite perpendicular to the magnetic field over Tromso for S94, also ram direction suitable for S80 when perigee near N. Pole.

III

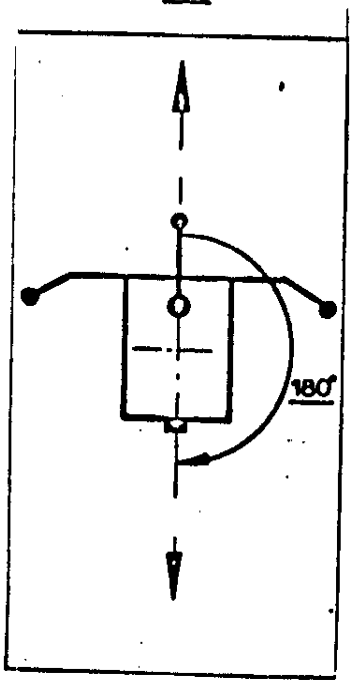

3. S80 ram direction over equator when perigee near descending node. Also S99 viewing out at S. Pole, S103 at N. Pole

IV

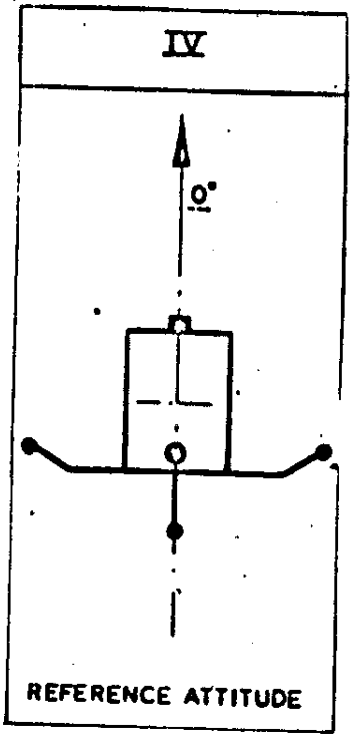

4. S80 ram direction over equator when perigee near ascending node. Also S99 viewing out at N. Pole, S103 at S. Pole.

V

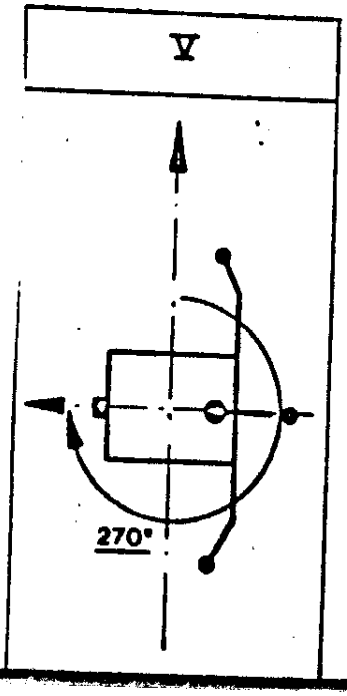

5. Designed to give good S80 dat when perigee is over the N. Pole.

(Additional attitude - 6 sometimes used when manoeuvering which is as 5. but spin axis turned through 180° - i.e. S80 data when perigee over S. Pole)

Manoeuvre No.	Start		Stop		Attitude	
	Orbit	Date/Time	Orbit	Date/Time	From	To
1	105	29/11/72	166	3/12/72	L	5
2	402	20/12/72	478	25/12/72	5	4
3	928	24/1/73	993	29/1/73	4	1A
4A	1566	9/3/73 09.31	1595	11/3/73 00.37	1A	6
4B	1610	12/3/73 22.01	1654	15/3/73 21.44	6	
4C	1669	16/3/73 21.58	1713	19/3/73 21.21		5
5	1934	3/4/73 20.23	1979	6/4/73 15.06	5	4
6	2556	15/5/73 06.41	2616.	19/5/73	4	6
6A	2660	22/5/73	2705	25/5/73 06.40	6	3
7	3181	26/6/73			3	5
8*	3494	17/7/73			5	4
9*	4019	21/8/73			4	3

* Confirmation of these dates not received at present

Appendix IV

Vector Manipulation for correcting spin modulation

Definition of the G.E.I. reference frame.

The origin is taken as the centre of the earth, the X direction is taken as the first point of Aries, the Z being perpendicular to the plane of the ecliptic to the north celestial pole and the y axis completes a right handed set of cartesian axes.

Then for every satellite data format (4.8 seconds) the following vectors in G.E.I. are known.

a) sun vector, $\underline{S}_{GEI}$

b) magnetic field vector, $\underline{B}_{GEI}$

c) satellite velocity vector, $\underline{V}_{GEI}$

d) spin axis vector, $\underline{SA}_{GEI}$

To enable the induced $\underline{V} \times \underline{B} \cdot \underline{L}$ potential on the probe to be calculated the boom position vector in G.E.I. must be known. The satellite in question spins about an axis which is parallel to the spin axis vector. A spin rate of approx. 1 r.p.s. and voltage sweep duration of 10 seconds are the two important time periods. Thus the spin modulation for a sweep is of the order of 10 cycles, this is clearly illustrated on Fig. 8.

Before setting up the necessary transformation from the centre of the satellite frame, in which the boom spins, to G.E.I. a number of approximations are made.

1) Over the duration of a sweep the spin axis vector remains constant.

2) The sun sensor placed on the satellite sees the sun every 360° of rotation. This holds good because in a spin period the satellite can be regarded as stationary relative to the sun. Hence, we can regard sun sensor period equivalent to the spin rate.

3) Using the fact that the satellite-earth distance is very small compared to the earth-sun distance assume that the sun vector in G.E.I. is the same as the satellite-sun vector in G.E.I.

The problem now reduces to the point where the satellite can be regarded as spinning at the G.E.I. origin about the spin axes. Then the sun vector, which is known in the satellite frame and G.E.I. frame is used to get the spin phase between the two frames correct. Define the satellite frame as having its Z axis along the spin axis and a X,Y plane that contains both the sun sensor and boom. A general cartesian transformation between the two frames can be achieved by using two angles P and Q. P is a positive rotation about the G.E.I. Z axis and Q a positive rotation about the new X axis.

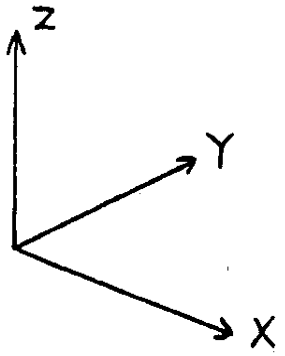

G.E.I.

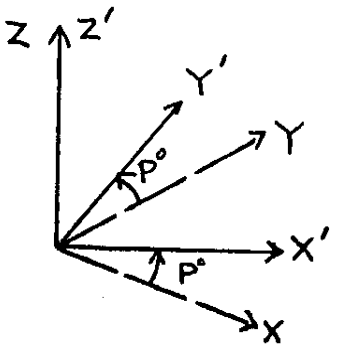

rotate by P

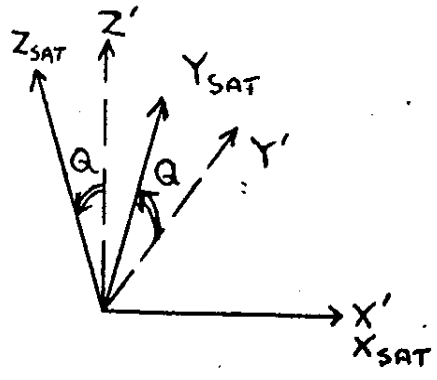

rotate by Q
to get satellite frame

Writing this in matrix form

$$\underline{R}_{GEI} = \begin{bmatrix} \cos P & -\sin P & 0 \\ \sin P & \cos P & 0 \\ 0 & 0 & 1 \end{bmatrix} \begin{bmatrix} 1 & 0 & 0 \\ 0 & \cos Q & -\sin Q \\ 0 & \sin Q & \cos Q \end{bmatrix} \underline{R}_{SAT}$$

$$= \begin{bmatrix} \cos P & -\cos P \sin Q & \sin P \sin Q \\ \sin P & \cos P \cos Q & -\sin Q \cos P \\ 0 & \sin Q & \cos Q \end{bmatrix} \underline{R}_{SAT}$$

$$= A \, \underline{R}_{SAT}$$

To evaluate the components of the transformation matrix A the spin vector, which is common to both frames, is used.

$$\underline{SA}_{GEI} = (SAx, SAy, SAz)$$

$$\underline{SA}_{SAT} = (0, 0, 1)$$

$\Rightarrow$ SAx = sin P sin Q, SAy = -sin Q cos P, and SAz = cos Q

hence we can find coefficients of A in terms of known vector components. The sun sensor sees the sun at a time T_o so that by transforming the Sun vector from G.E.I. to the Satellite frame the sun sensor position is known. However, since the rotation is about the z axis the position of the sensor in the spin plane (x,y) is required. This is obtained by projecting the sun vector in the satellite frame on to the x,y plane. The position in the x,y plane is given by an angle R as follows.

$$\underline{S}_{SAT} = A^T \underline{S}_{GEI}$$

$$\underline{S}_{SAT} = (Sx, Sy, Sz)$$

$$\tan R = \frac{Sy}{Sx}$$

hence the sun sensor position at a subsequent time t is given by:

$$x = \cos (w (t - T_o) + R)$$

$$y = \sin (w (t - T_o) + R)$$

where w is the spin rate. The boom is at a further 100^o in the positive rotation sense to the sun sensor.

$$\therefore x_{BOOM} = \cos (w (t - T_o) + R + 100)$$

$$y_{BOOM} = \sin (w (t - T_o) + R + 100)$$

Then the third component z_{BOOM} is set to 0. In actual fact the boom ends are tilted at 17^o to the spin plane. Now the transformation A can be used on $\underline{L}$ satellite, stated in component form above, to obtain the required G.E.I. boom position vector.

$$\underline{L}_{GEI} = A \, \underline{L}_{SAT}$$

Thus by making use of the given $\underline{B}_{GEI}$ and $\underline{V}_{GEI}$ vectors the voltage induced on the boom can be calculated by evaluating the vector expression

$$\underline{V}_{GEI} \times \underline{B}_{GEI} \cdot \underline{L}_{GEI}$$

giving the scalar potential induced on the boom.

Appendix V

Reduction of Electron Probe Data to Geophysical Parameters

The programmes to date have used the straightforward electron Langmuir probe theory for spherical probes using the following relations:

In retarding region $$i = i_o e^{-\frac{|V|}{kT}} \quad \ldots\ldots\ldots 1.$$

where
- i_o = probe current when V = 0
- V = probe - plasma potential
- k = Boltzmann's Constant
- T = electron temperature

In accelerating region $$\frac{di}{dV} = \left|\frac{di}{dV}\right|_{V=0} = \frac{i_o}{kT} \quad \ldots\ldots\ldots 2.$$

The current to the probe at plasma potential is given by

$$i_o = \tfrac{1}{4} A e n \left(\frac{8kT}{\pi m}\right)^{\frac{1}{2}} \quad \ldots\ldots\ldots 3.$$

where
- A = probe area
- e = electronic charge
- n = electron density
- m = electron mass

We can deduce the electron temperature from 1. as follows:-

$$\left|\frac{di}{dV}\right| = \frac{i_o}{kT} e^{-\frac{|V|}{kT}}$$

$$\therefore \quad \ln\left|\frac{di}{dV}\right| = -\frac{V}{kT} + K \quad \ldots\ldots\ldots 4.$$

The experiment measures a parameter which is dependant on the $\log\left|\frac{di}{dV}\right|$ in the following way:-

$$\frac{i_{ac}}{v_{ac}} \approx \frac{di}{dV}$$

where
- i_{ac} = ac current flowing in probe
- v_{ac} = ac voltage applied to probe

We measure i_{ac} in db

$$\text{i.e.} \quad db = 20 \log \left(\frac{i_{ac}}{i_{ref}} \right)$$

$$\therefore \log i_{ac} = \frac{db}{20} + \log \left(i_{ref} \right)$$

$$\therefore \log \left(\frac{di}{dV} \right) = \log(i_{ac}) - \log(V_{ac})$$

$$= \frac{db}{20} + \log(i_{ref}) - \log(V_{ac}) \quad \ldots. \; 5.$$

but from 4.

$$\log \left| \frac{di}{dV} \right| = \frac{-V}{\ln 10 \, . \, (kT)} + K' \quad \ldots. \; 6.$$

Equating 5. & 6.

$$\frac{db}{20} + \log(i_{ref}) - \log(V_{ac}) = \frac{-V}{\ln 10 \, . \, (kT)} + K' \quad \ldots. \; 7.$$

From 4. we can see that it is the derivative of $\left| \frac{di}{dV} \right|$ wrt V which is a measure of T, thus if we differentiate 7. wrt V we can obtain an expression for the relation between the slope of the measured signal in db/volt to the electron temperature.

Substitution of constants gives

$$T = \frac{1.00803 \times 10^5}{S} \quad \ldots. \; 8.$$

Where S is the slope of the retarding region of the characteristic expressed in db/volt.

Having ascertained T we can then use equation 2, and 3. to deduce the electron density n.

$$\left| \frac{di}{dV} \right|_{V=0} = \frac{\frac{1}{4} A e n \left(\frac{8k}{\pi m} \right)^{\frac{1}{2}} \, . \, T^{\frac{1}{2}}}{kT}$$

Note in substituting for the constants the 'k' in the numerator is in J deg^{-1}, while in the denominator it is in eV deg^{-1}.

Substituting for the constants gives

$$\left| \frac{di}{dV} \right|_{V=0} = 9.0717 \times 10^{-16} \left(\frac{n}{T^{\frac{1}{2}}} \right) \quad \ldots. \; 9.$$

Where n is in m^{-3}

and T in degrees Kelvin

The determination of S and $\left|\frac{di}{dV}\right|_{V=0}$ is made in the subroutine DEKINK. This subroutine selects the data for curve fitting also sets up the data to fit a straight line plus a spin modulation component in the subroutine SPINLN.

Let E be the experimental db value of i_{ac}, then in the retarding region, from equation 7., we wish to fit the function

$$E = \alpha V_{ps} + \beta \quad \ldots\ldots 10.$$

Where V_{ps} = probe to spacecraft ground voltage

(Note the constant bias due to the spacecraft-plasma potential can be ignored in this application because it has been taken care of in the way in which the data has been selected to be in the retarding region. Mathematically it would represent part of the constant β in 10.)

Now V_p is made up of a bias voltage generated by the sweep voltage generator (V_p), and an induced voltage due to the v x B potential along the boom. The latter can be represented as the sum of a sine and cosine term to represent an orbitary amplitude and phase.

$$\therefore V_{ps} = V_p + (a \sin \omega t + b \cos \omega t)$$

ω = satellite spin rate

V_p = Voltage output of sweep generator

$$\therefore E = \alpha V_p + \alpha a \sin \omega t + \alpha b \cos \omega t + \beta$$

$$\text{or } E = A + BV_p + C \sin \omega t + D \cos \omega t \quad \ldots\ldots 11.$$

Where B = slope in db/volt

$$a = \frac{C}{B}, \quad b = \frac{D}{B}$$

We may fit such a function by the method of least squares which is done in SPINLIN by forming the coefficients of the four simultaneous equations generated and solving them by use of the IBM/SSP routine SIMQ.

The value of B deduced may then be used in 8. to obtain the electron temperature. The values of a and b enable the spin modulation correction to be made for S45/1 when the satellite is in darkness.

The electron density is computed from the maximum value of $\frac{di}{dV}$ which generally occurs near space potential.

The actual space potential is deduced by finding the intersection of the non-oscillating part of 11. with the line.

$$\left|\frac{di}{dV}\right|_{max} = \text{const.}$$

Contents of OUT (I,1), I=1, 25

I	Contents
1	Julian Day number, origin 1950.00
2	Day of Month
3	Number of Month
4	Year
5	HH } Time origin of pass (U.T.)
6	MM } Time origin of pass (U.T.)
7	SS } Time origin of pass (U.T.)
8	Orbit Number
9	Sidereal angle (deg. x 10^{-1})
10	Spin axis X } Normalised to 10^4 (GEI)
11	Spin axis Y } Normalised to 10^4 (GEI)
12	Spin axis Z } Normalised to 10^4 (GEI)
13	Spin rate deg. x 10^{-1}/sec
14	Sun Vector X } Normalised to 10^4 (GEI)
15	Sun Vector Y } Normalised to 10^4 (GEI)
16	Sun Vector Z } Normalised to 10^4 (GEI)
17	S45/1 8.5 kHz amplitude (mV)
18	S45/1 10.5 kHz amplitude (mV)
19	Positive 6 volt monitor (mV)
20	Preamp. Temperature (deg. x 10^{-1})
21	Negative 6 volt monitor (mV)
22	Package Temperature (deg. x 10^{-1})
23	Bias voltage (mV)
24	S45/2 3.2 kHz amplitude (mV)
25	Spare

Contents of OUT (I,J), I = 1,25, J = 2, NSW

I	Contents
1 I5	Amplitude of light ion peak (amps x 10^{-11})
2 I6	Voltage of light ion peak (mV)
3 I5	Amplitude of heavy ion peak (amps x 10^{-11})
4 I6	Voltage of heavy ion peak (mV)
5 I6	Electron Temperature (deg.K)
6 I4	Electron Density (cm^{-3} x 10^{2})
7 I5	Space Potential (mV)
8 I5	Elapsed Orbital time of sweep (at VSP) (secs)
9 I5	S45/3 current (μA)
10 I6	S45/3 fluctuations spin modulation amplitude
11 I6	S45/3 fluctuations derived scale height
12 I6	S45/3 rms deviation of fit
13 I5	Longitude (deg. x 10^{-1})
14 I5	Latitude (deg. x 10^{-2})
15 I6	Altitude (km x 10^{-1})
16 I6	Angle of Attack of Spin Axis (deg. x 10^{-2})
17 I5	Invariant Latitude (deg. x 10^{-2})
18 I5	Velocity (m/s)
19 I5	Experiment Status (coded)
20 I4	Kp at sweep time (ESOC code)
21 I5	Temperature of 0^{+} ion (deg. K)
22 I5	Density of 0^{+} ion (cm^{-3} x 10^{3})
23 I4	Temperature computation status flag
24	Spare
25 I2	Sunlight/Darkness Flag

Definition of Status Flags

1. OUT (19,N)

This number is computed as follows:-

1000*KSENS + 100*IVCOR + 10*STATB(4) + 4*STATB(3) + 2*STATB(2) + STATB(1)

Where

KSENS is S45/1 sensitivity flag = 1 High sensitivity
= 2 Low sensitivity

IVCOR is S45/1 spin modulation correction flag
= 0 Correction by using attitude solution and spin phase monitor
= 1 Correction by fit to S45/2 data (used in darkness)

STATB(4) = 1 Experiment on
= 0 Experiment off

STATB(3) = 1 Bias = -10 volts
= 0 Bias = - 6 volts

STATB(2) = 1 Scanning sweep mode
= 0 Normal sweep mode

STATB(1) = 1 S45/1 ac voltages ≈ 200mV
= 0 S45/1 ac voltages ≈ 50mV

---

2. OUT (23,N)

This number is computed as:-

100*IVCOR + 10*MAD + KX

Where

IVCOR is S45/1 spin modulation correction flag
= 0 Correction using attitude solution and spin phase monitor
= 1 Correction by fit to S45/2 data

MAD = 0 Good fit to S45/2 data
= 1 Bad fit to S45/2 data

KX = 0 Peak not usable
= 1 Lower half width of 0^+ peak used
= 2 Upper half width of 0^+ peak used
= 3 Total width of 0^+ peak used

List of Figures

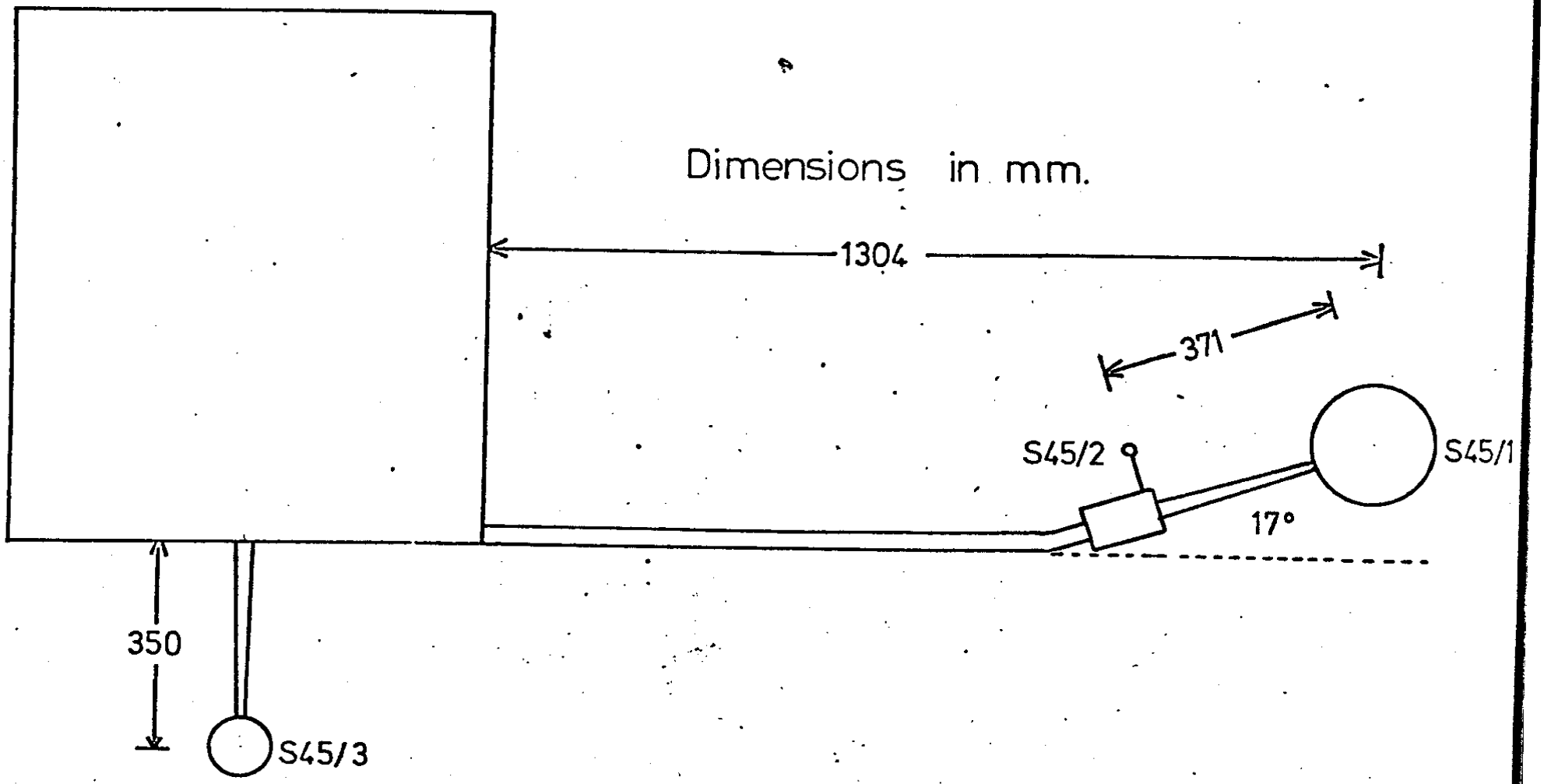

fig Schematic Diagram Showing Positions of S45 Probes

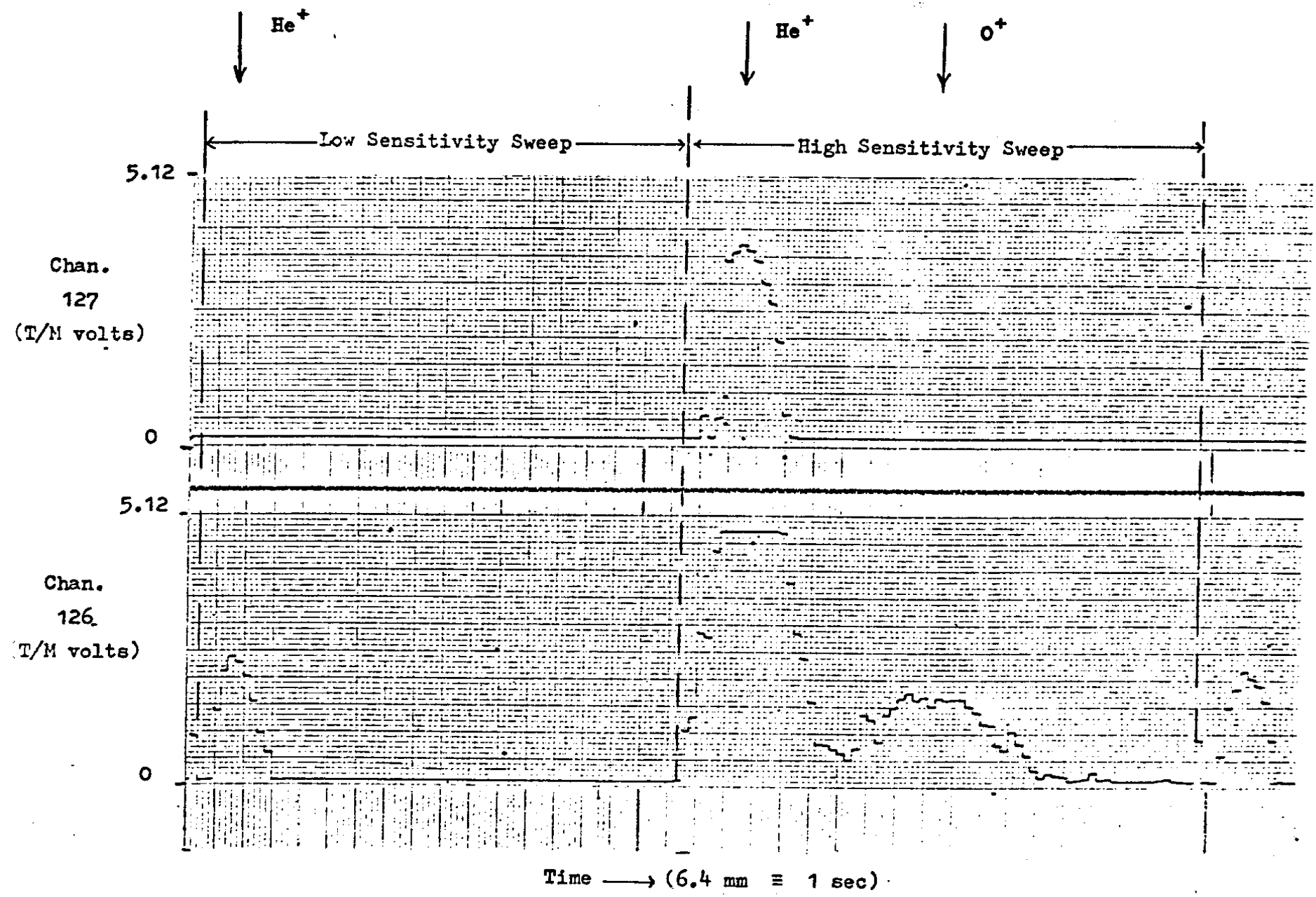

Orbit 824
18th Jan. 1973

Satellite in
attitude 4

fig 2. S45/1 Raw Data showing peaks in second derivative as He^+ and O^+ ions are retarded. Data taken over the magnetic equator

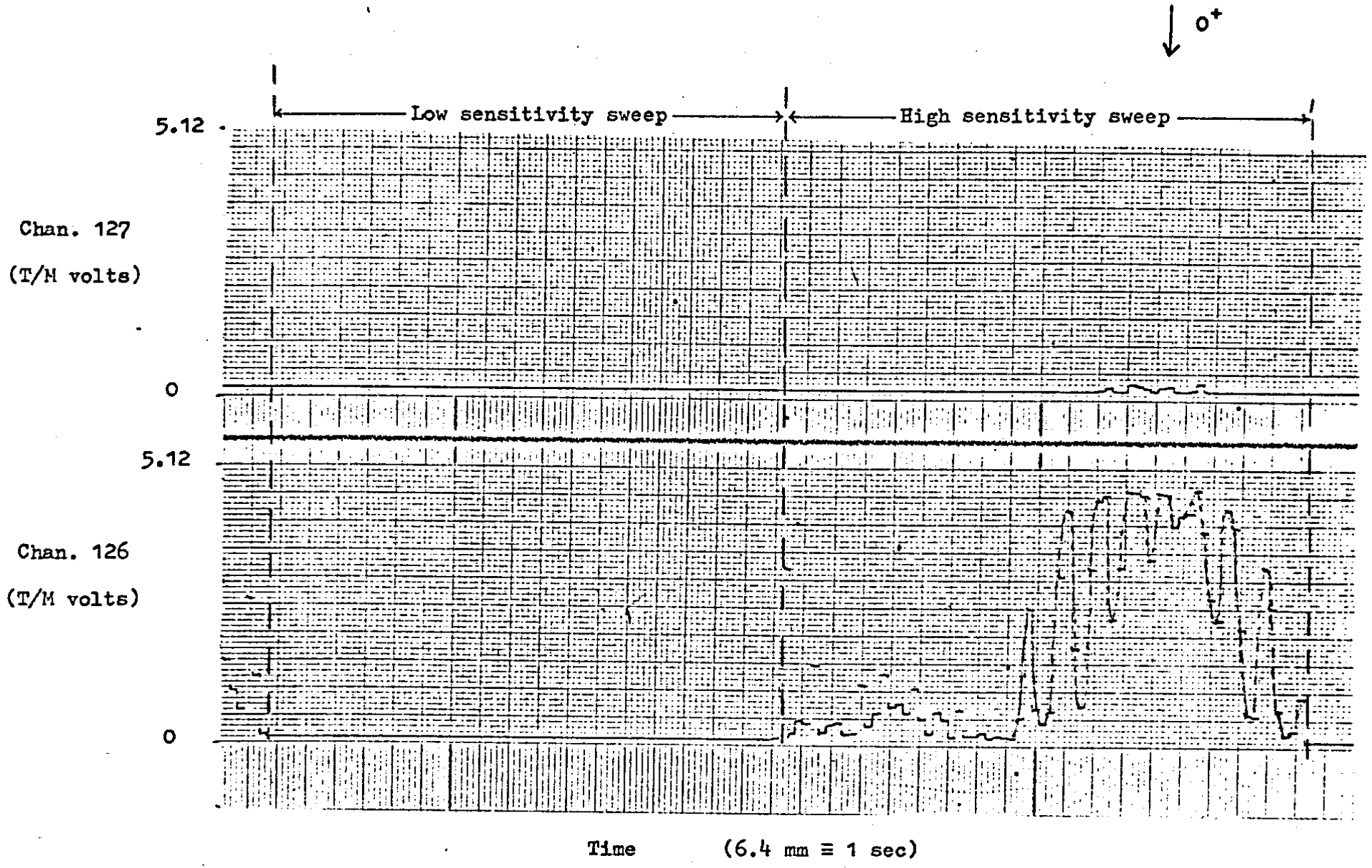

fig 3. Example of S45/1 raw data showing spin modulation due to v x B

Orbit 1000 29th Jan. 1973

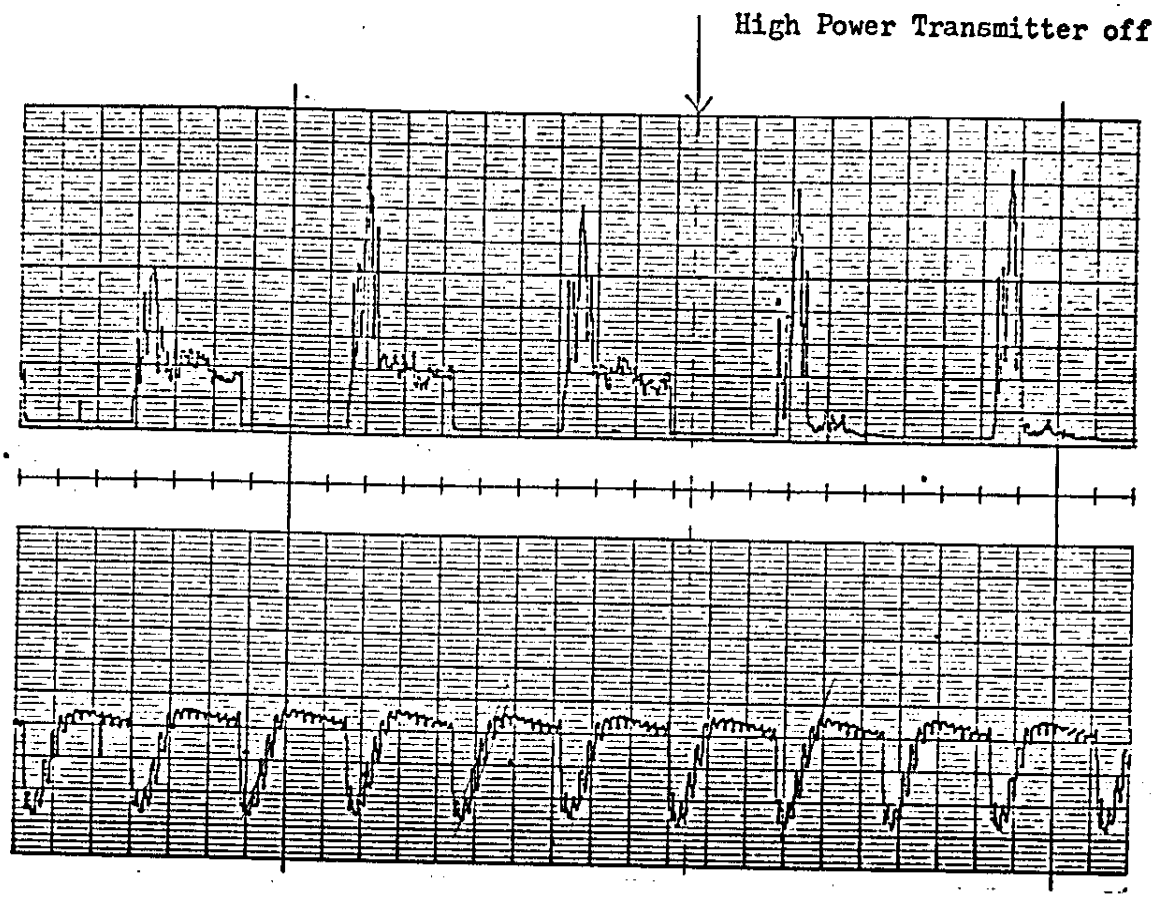

fig. 4 Interference to S45/1 data from High Power Transmitter

Orbit 2613 19th May 1973

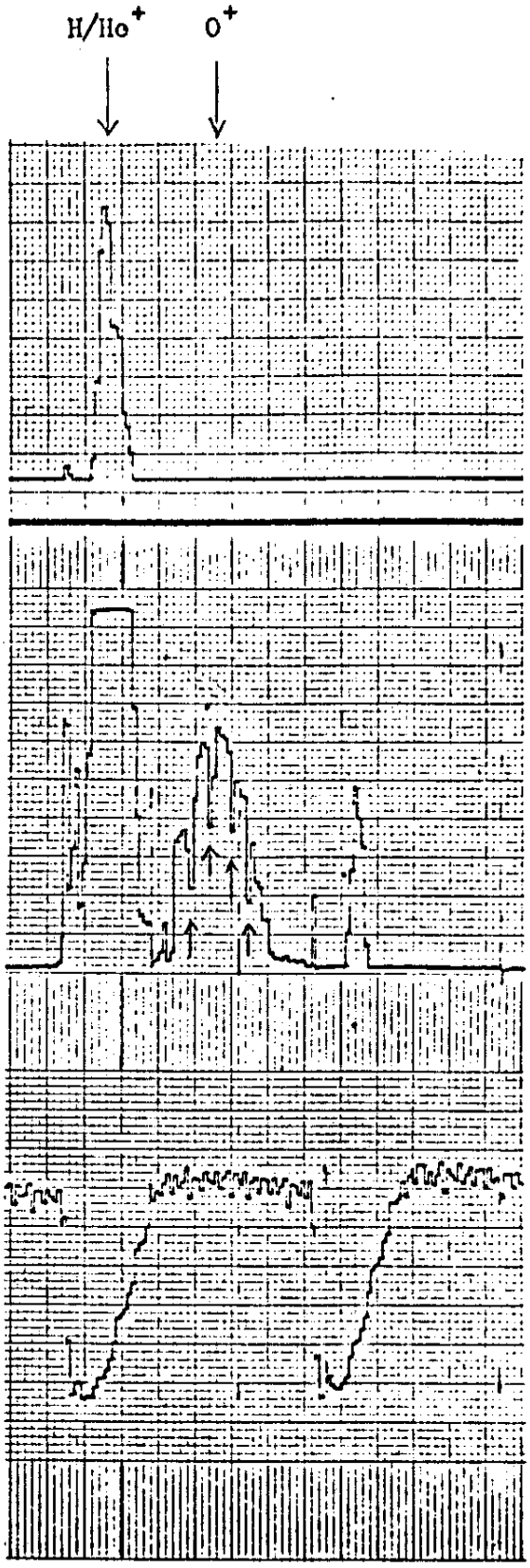

fig 5. Wake effect observed by S45/1 Probe

Orbit 824 (18th Jan. 1973) Attitude 4

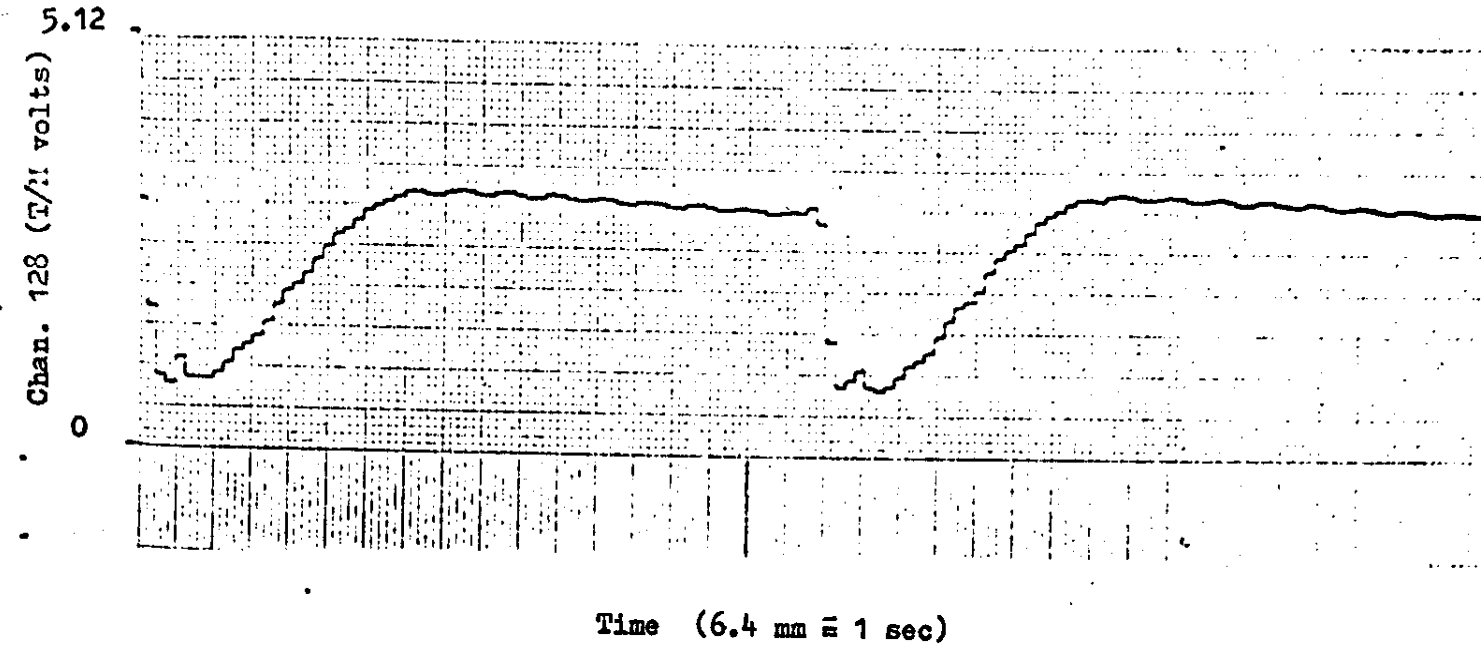

a) Data taken near equator when v x B tends to zero

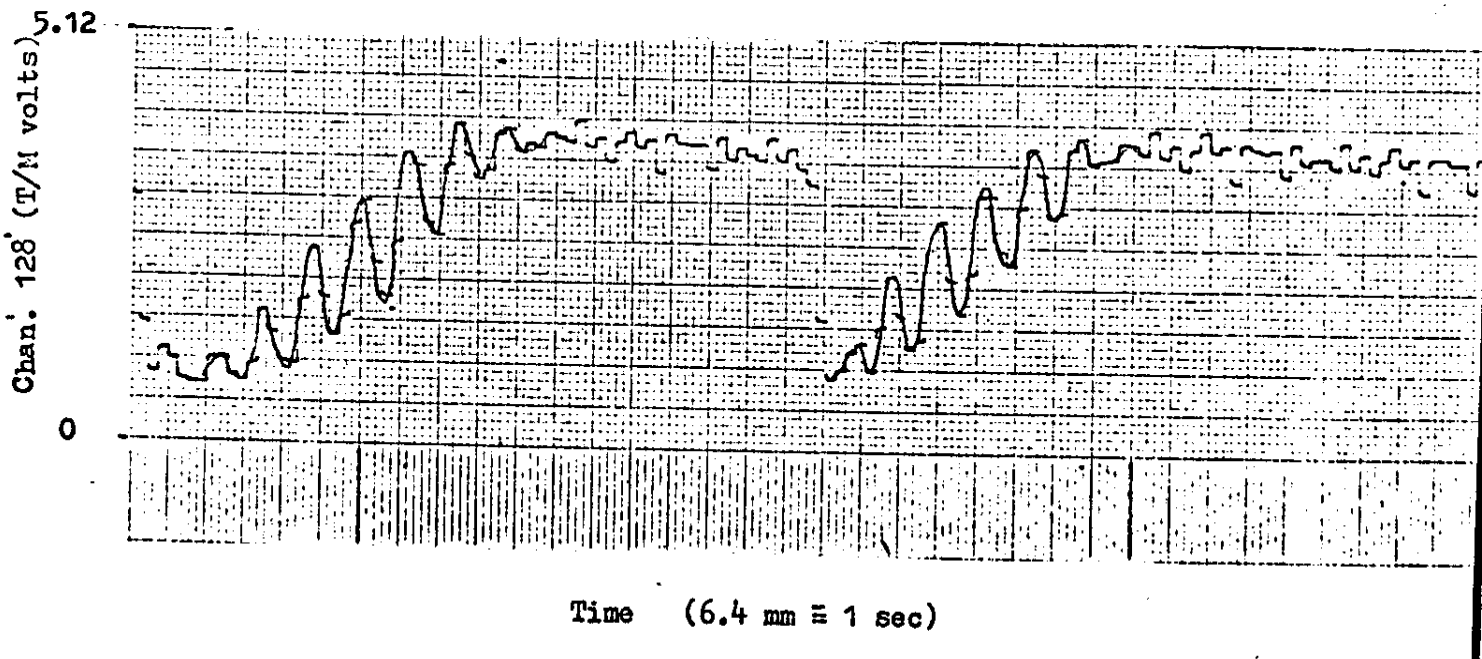

b) Data taken at higher latitude showing spin modulation

fig 6. Example of raw S45/2 Data

a) Undisturbed ionosphere showing regularly changing ion density

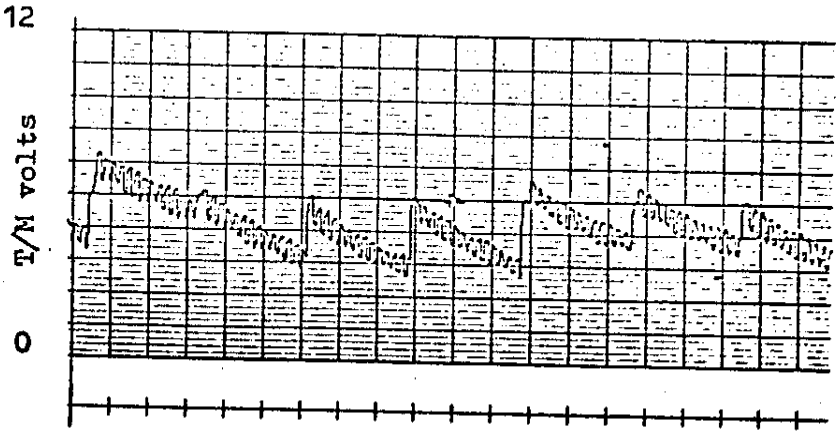

b) Disturbed polar region. Large amplitude rapid fluctuations. Arrows show reset times.

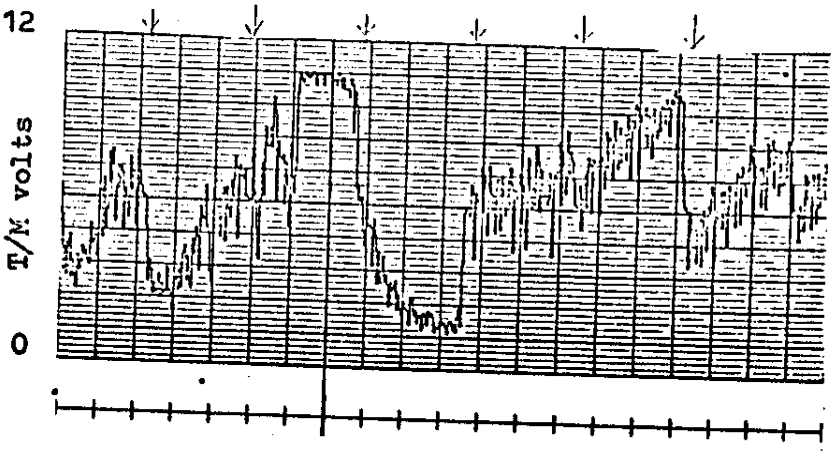

c) Spin rate modulation as S45/3 enters or leaves the wake of the satellite.

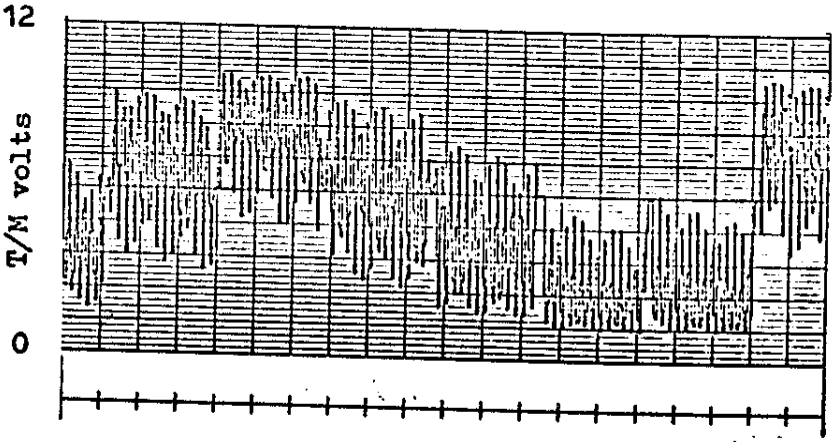

time (1.3 mm = 1 sec)

fig 7. Characteristic Forms of S45/3 Fluctuations Output

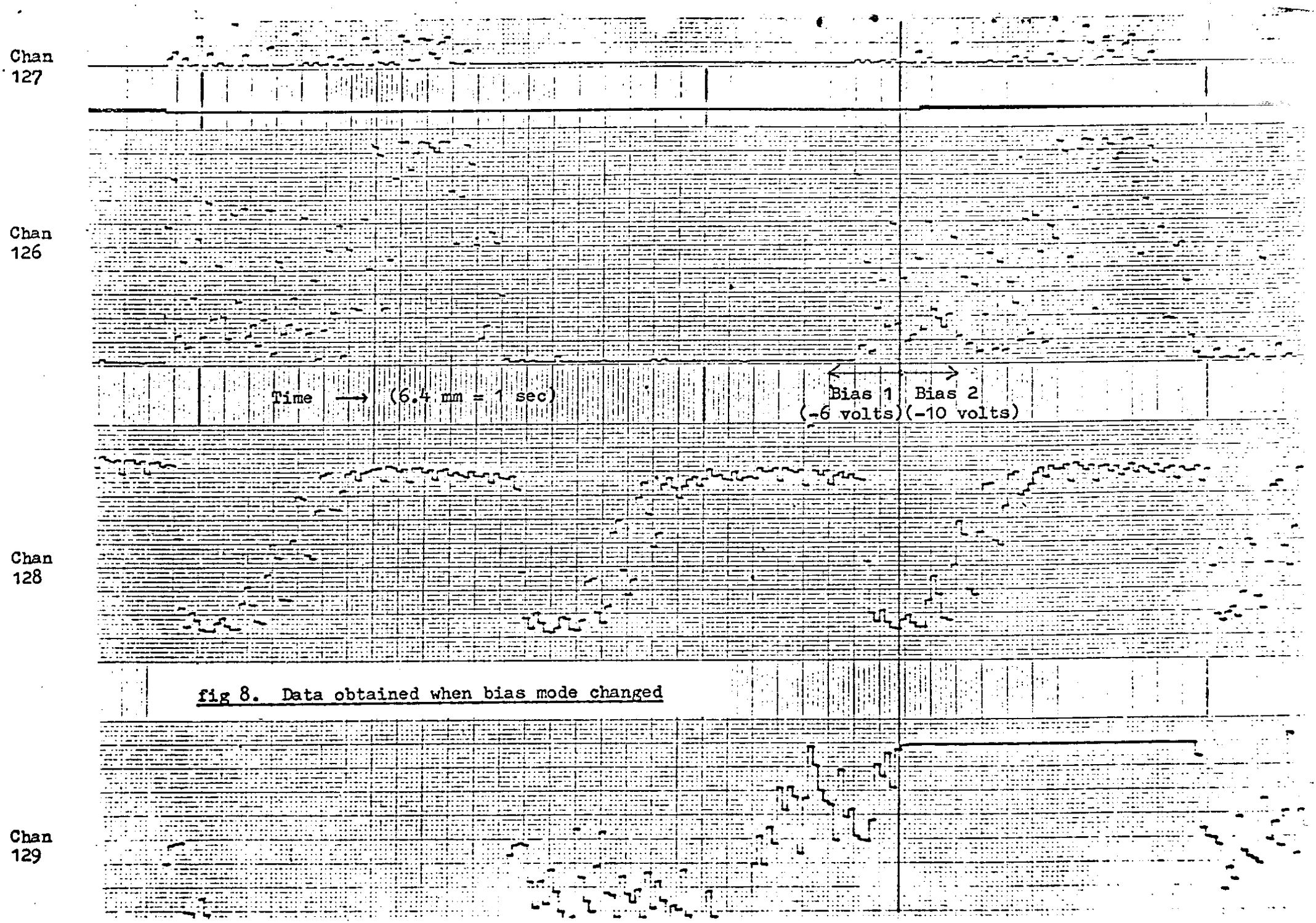

fig 8. Data obtained when bias mode changed

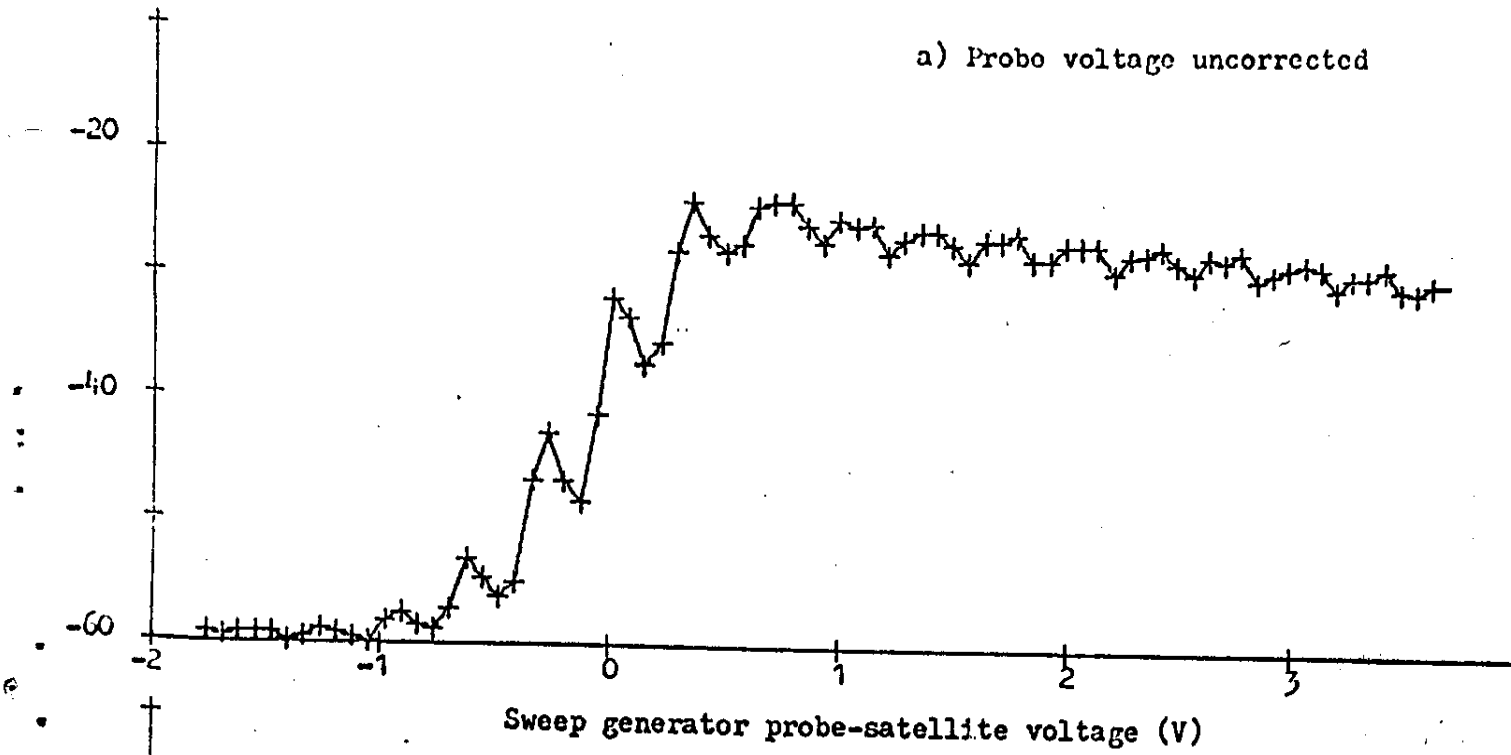
a) Probe voltage uncorrected
-20
-40
-60
-2
-1
0
1
2
3
Sweep generator probe-satellite voltage (V)

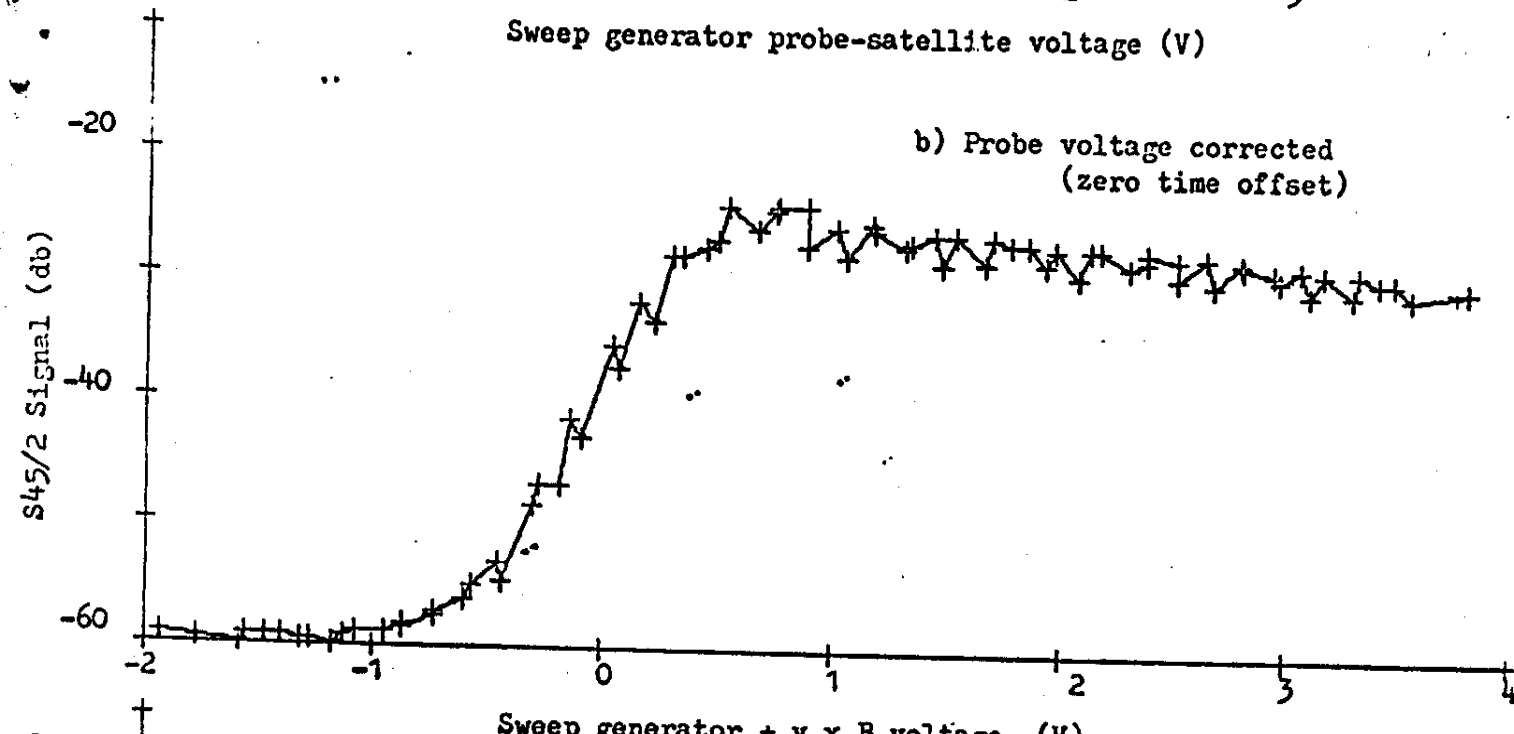
b) Probe voltage corrected
(zero time offset)
S45/2 Signal (db)
-20
-40
-60
-2
-1
0
1
2
3
4
Sweep generator + v x B voltage (V)

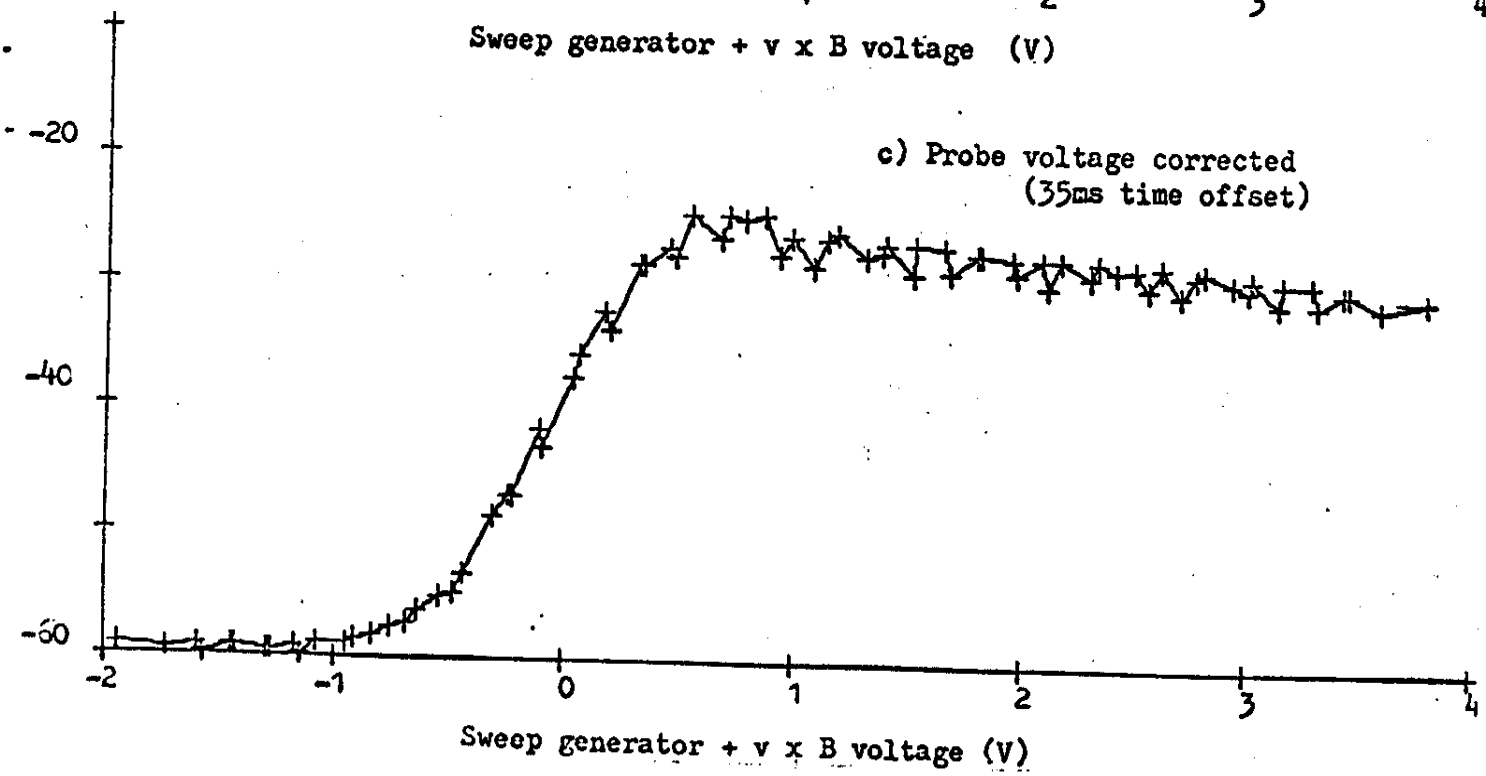
c) Probe voltage corrected
(35ms time offset)
-20
-40
-60
-2
-1
0
1
2
3
4
Sweep generator + v x B voltage (V)

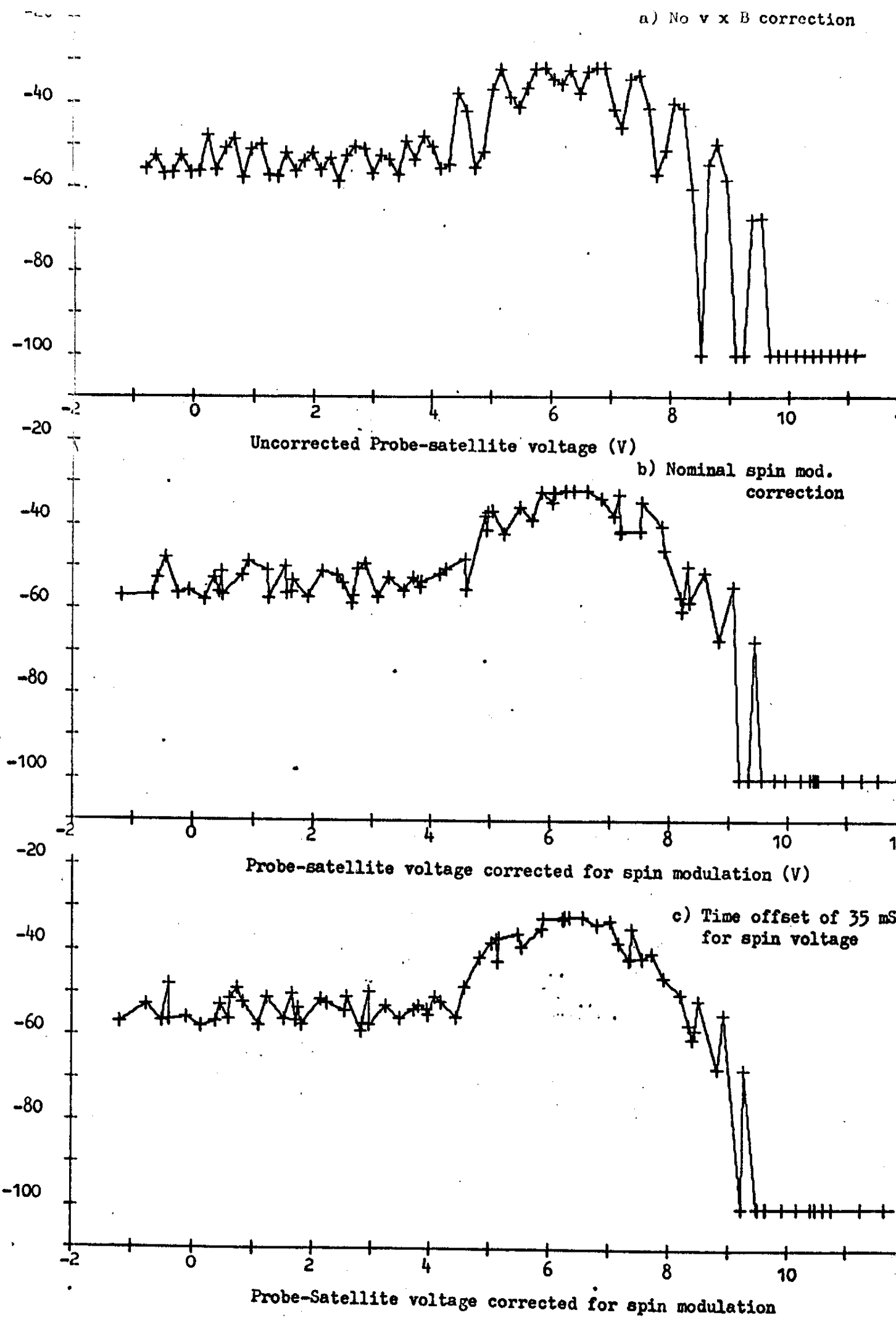

fig 10 Spin modulation correction for S45/1

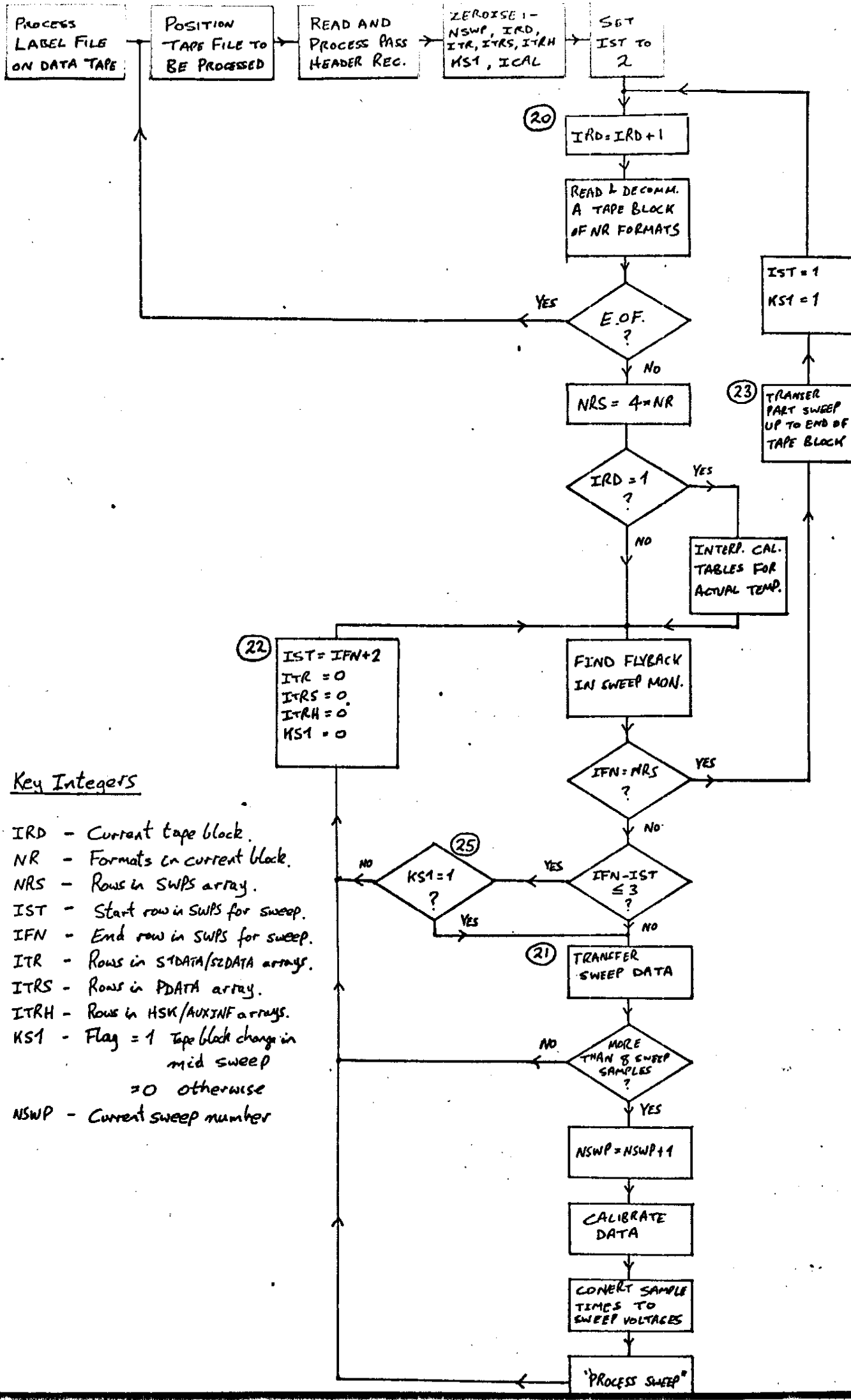

Key Integers

IRD - Current tape block.
NR - Formats on current block.
NRS - Rows in SWPS array.
IST - Start row in SWPS for sweep.
IFN - End row in SWPS for sweep.
ITR - Rows in S1DATA/S2DATA arrays.
ITRS - Rows in PDATA array.
ITRH - Rows in HSK/AUXINF arrays.
KS1 - Flag = 1 Tape block change in mid sweep
=0 otherwise
NSWP - Current sweep number

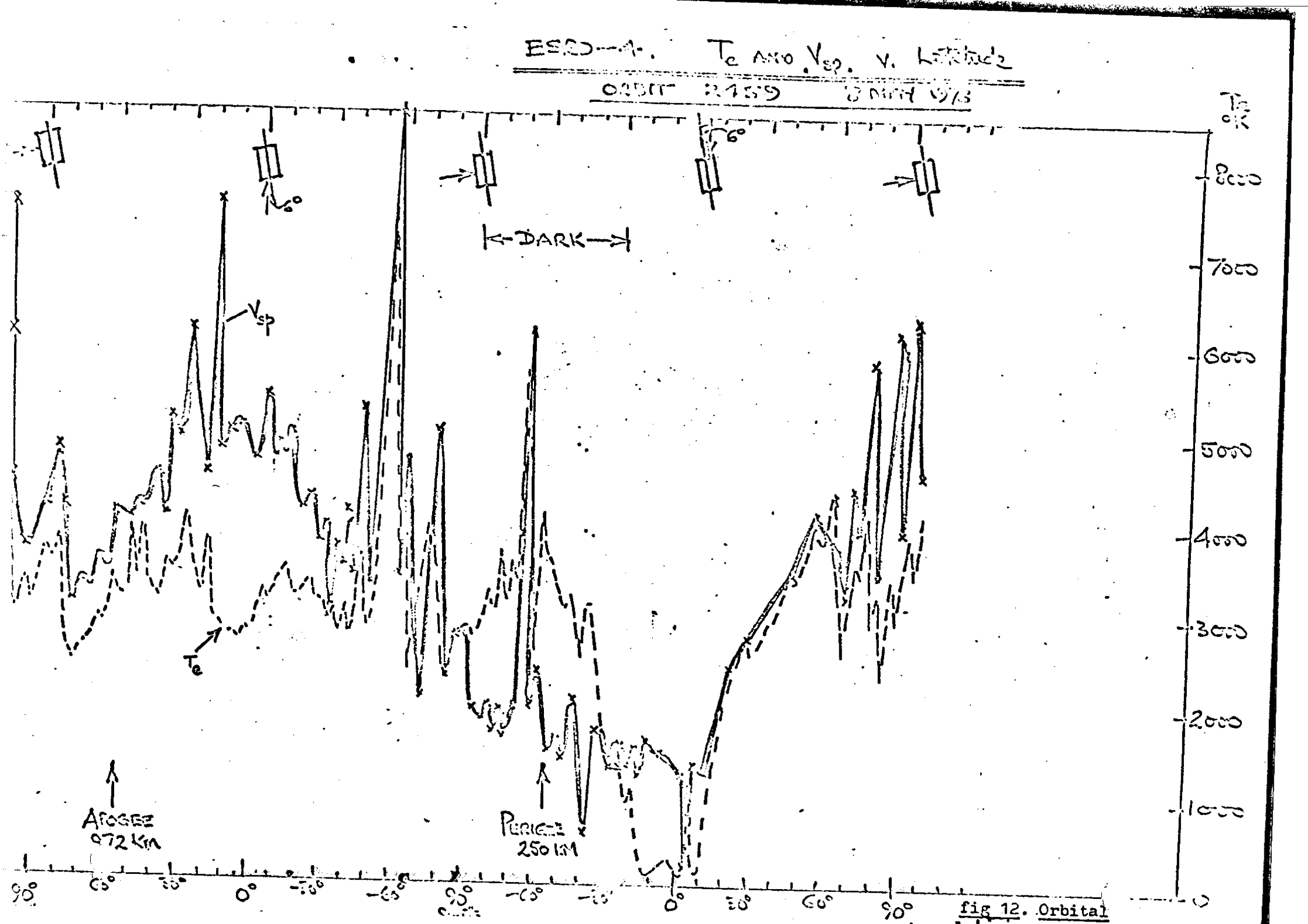

fig 12. Orbital

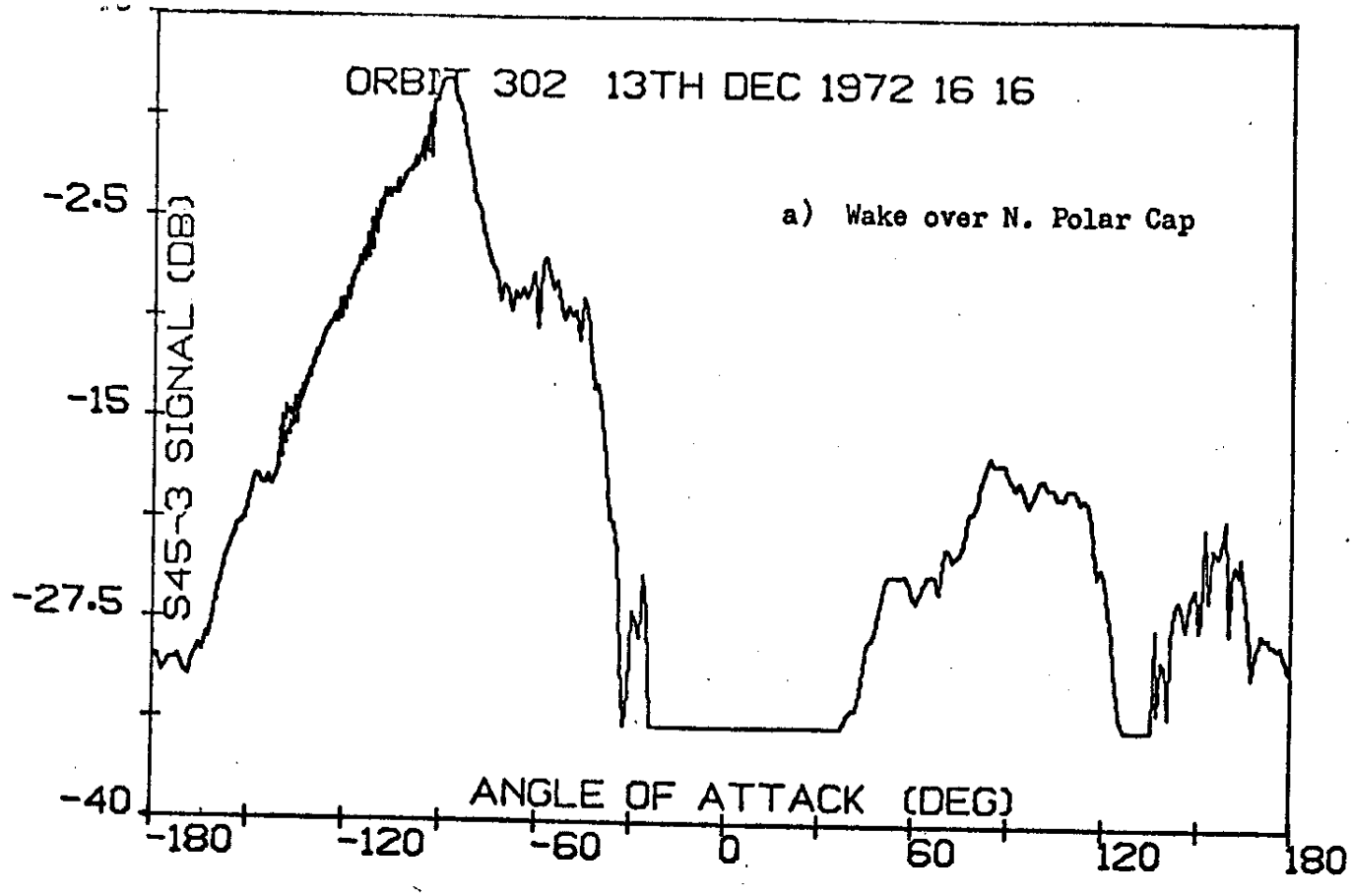

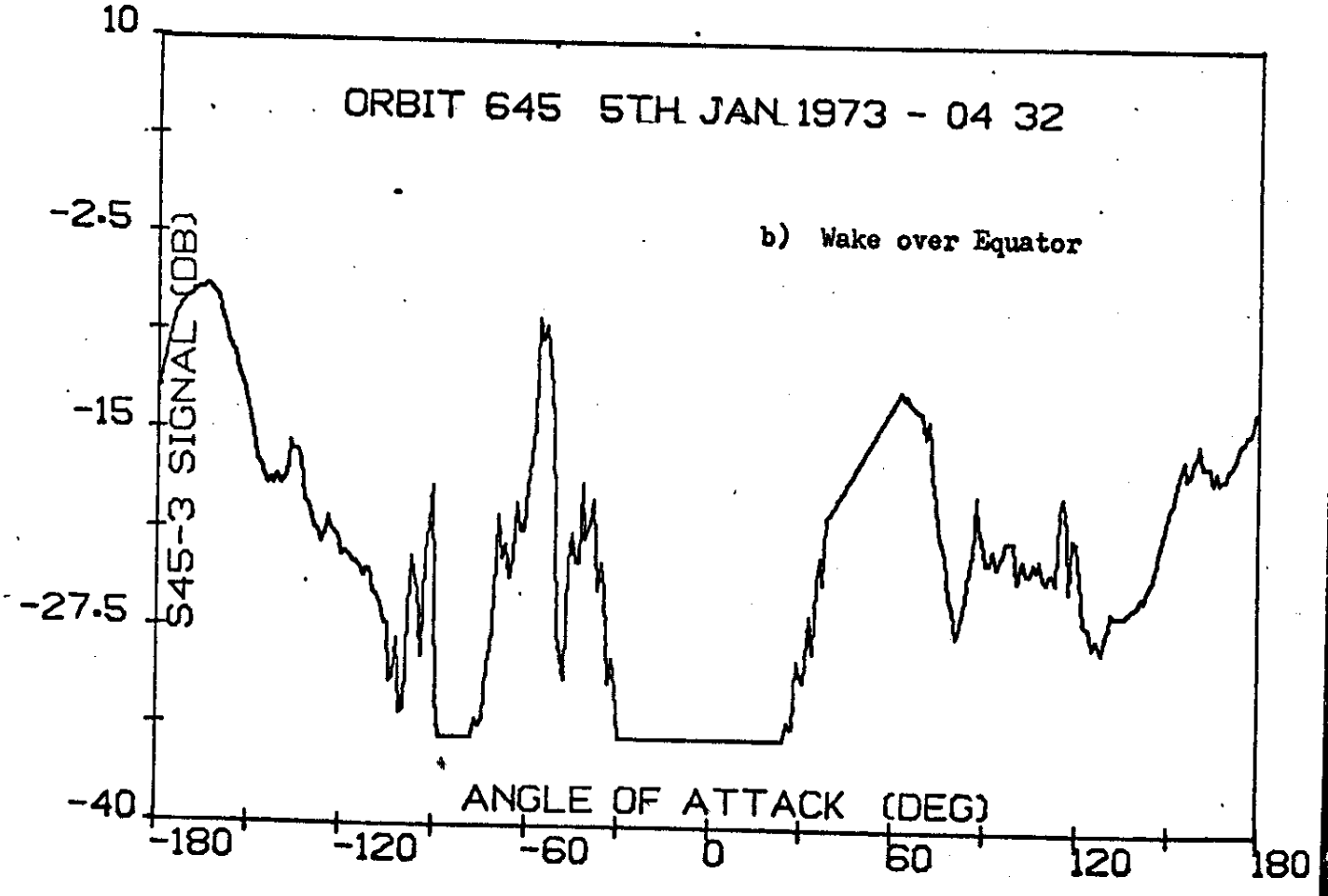

fig. 13 Plots of S45/3 data showing the satellite wake

S45/3 Spin Amp. v. Time Orbit 785 14-1-73

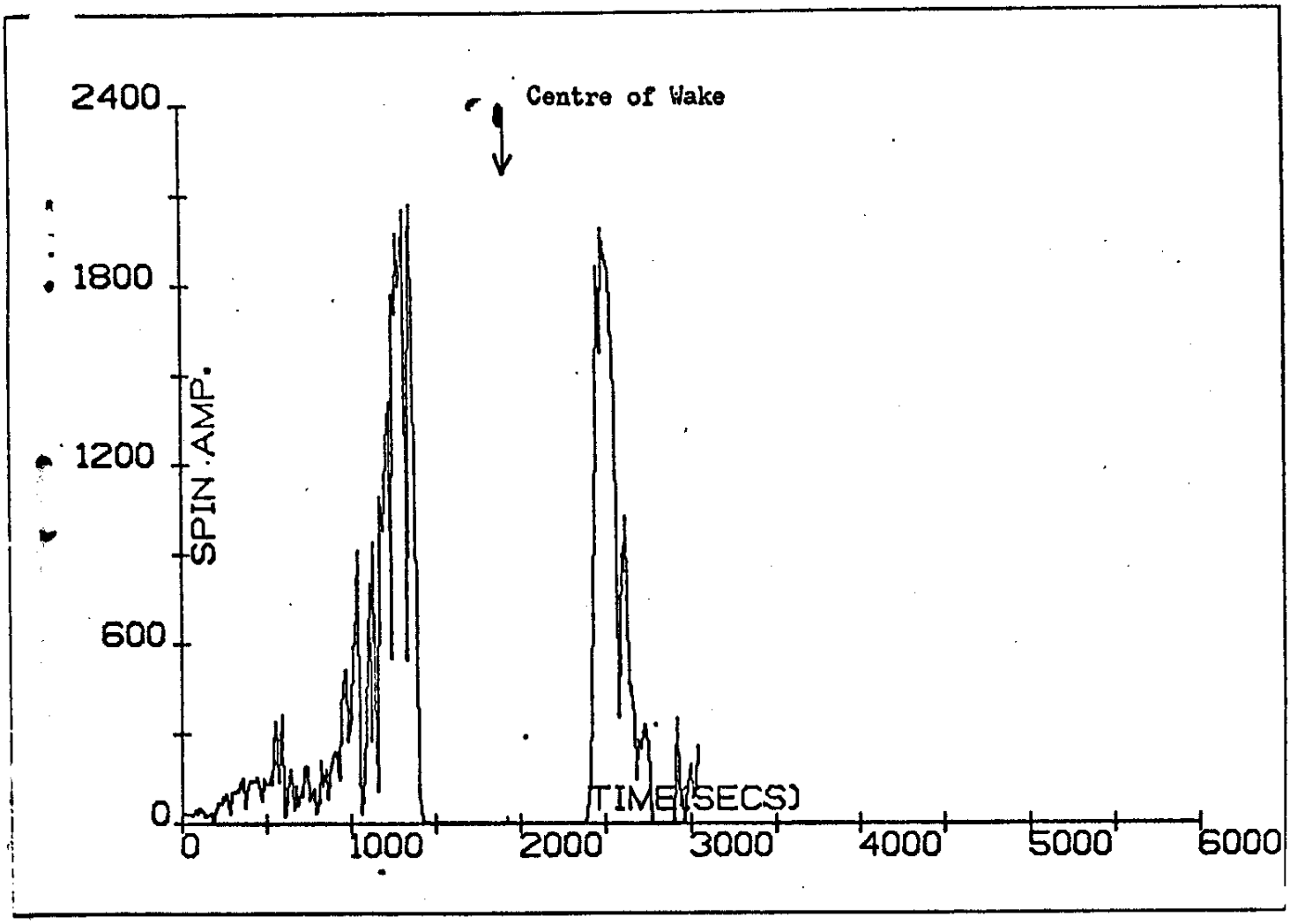

fig 14 Spin modulation on S45/3 fluctuations channel

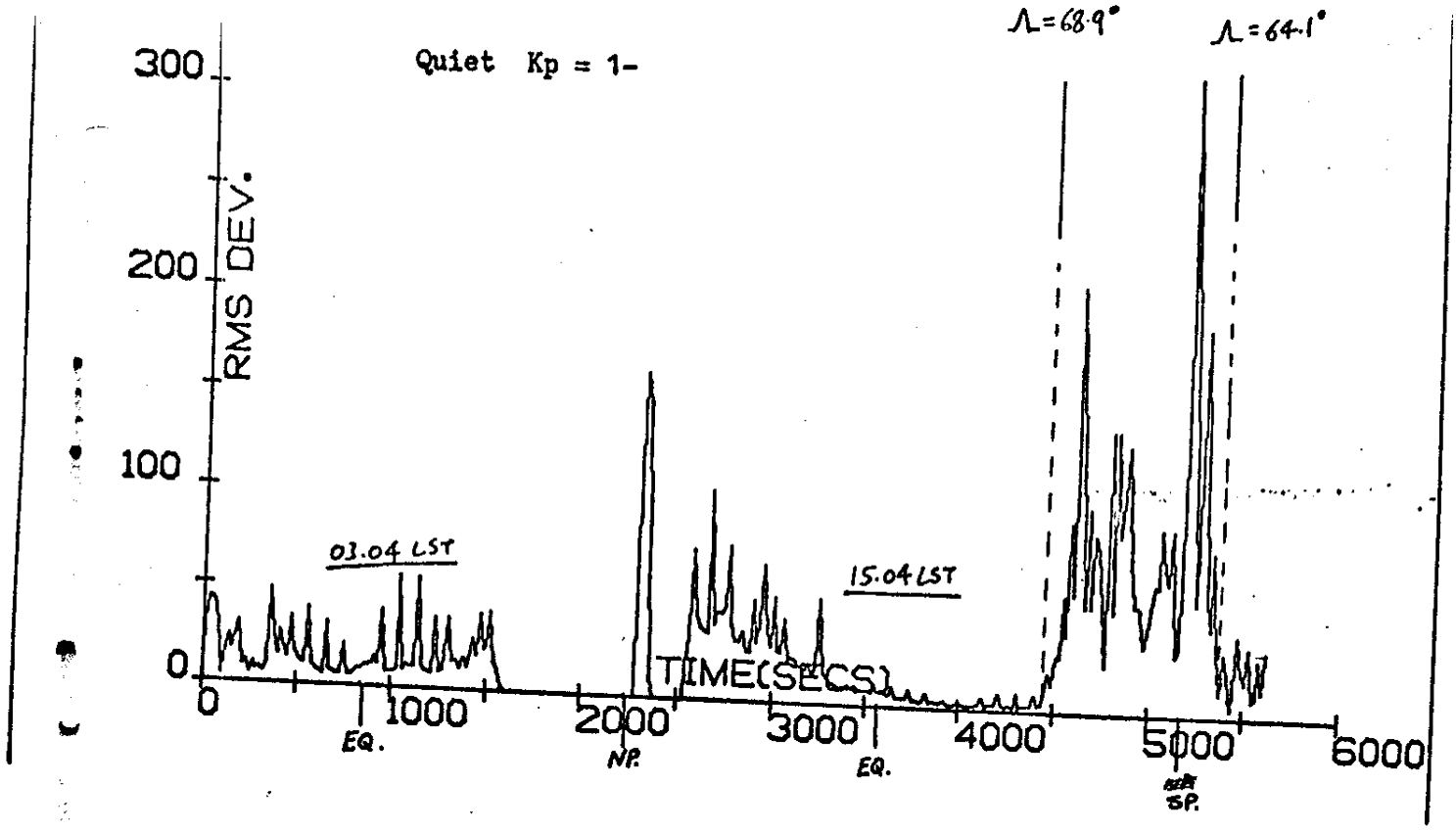

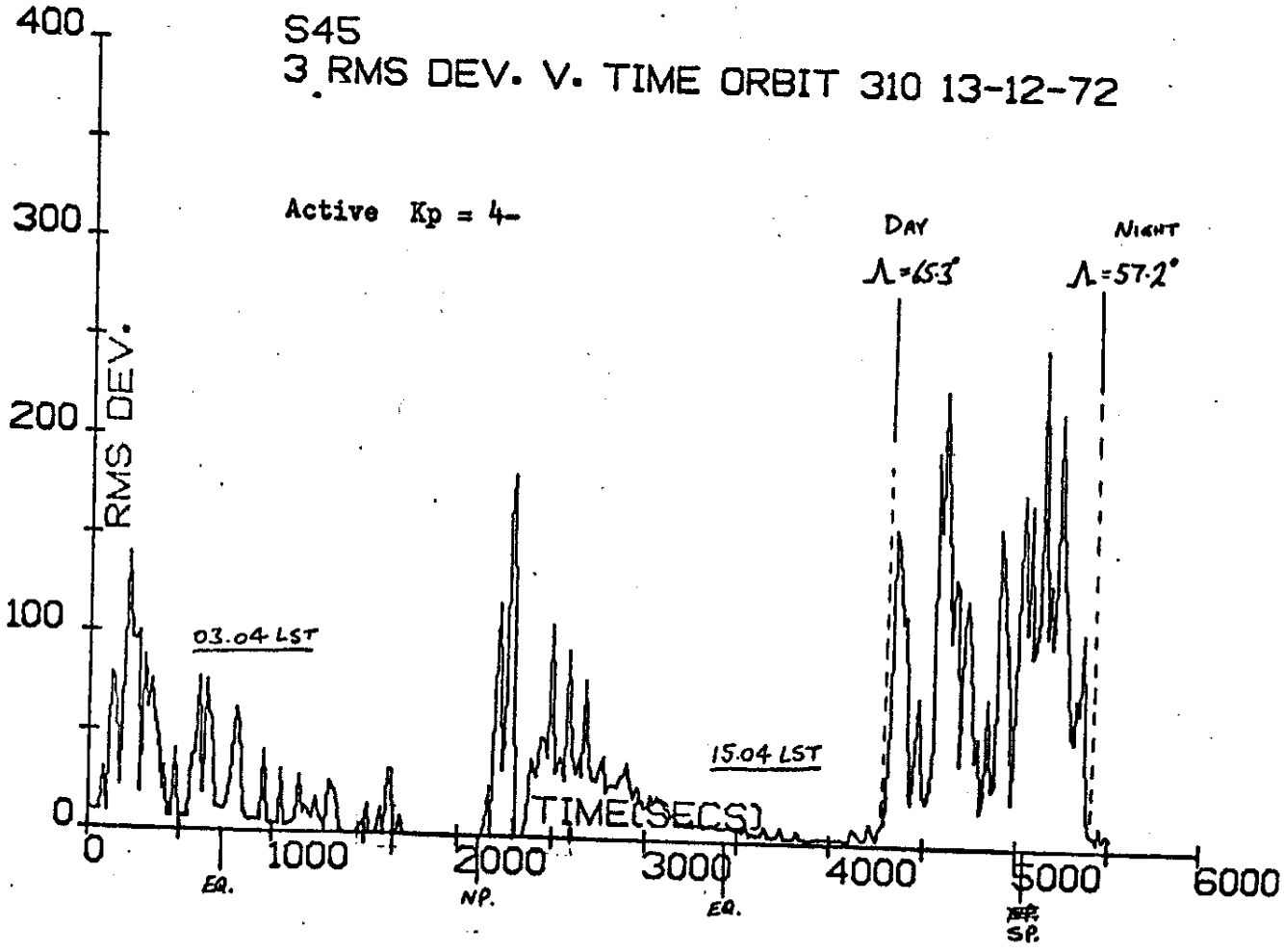

fig 15. Rms deviation showing particle precipitation boundaries at S.Pole

DUMP OF TAPE ~~X-429~~ D-30957 ESRO-4

D-30957

INPUT TAPE X-429 ON MS3
DATA INPUT H9 NF 1 FL 1 1 1

FILE 1 RECORD 1 LENGTH 14850BYTES

(0)	20A90016	000B07B4	00011002A	00050002	14870441	F333DB58	0F86EC58	E108F293	0C400CC	1733013E
(40)	E7A100E4	F4E9002B	00BB0000	0ECF0000	2C9FFFFF	FFFFFFFF	00000002	0000D8F0	0001014E	1E571DAB
(80)	1EE81CD7	1D2407DA	0014FFFF	FFFF000A	179A0001	0011101E8	000A11D2	15A1004D	046B000E	00020016
(120)	FA2F002B	014B1E90	1D7D1EAE	1D091D29	03F20014	FFFFFFFF	000017D5	00010000	FB590000	2C0DFFFF
(160)	FFFFFFFF	001E0002	00271B4C	004C0144	1F031D20	1E3B1D6C	1D3207DA	0014FFFF	FFFF000A	182E0001
(200)	0011027A	000C160E	0E5D0052	03320033	00020053	FF730067	013C1F76	1CC21DC7	1DCE1D3C	03F20014
(240)	018C0006	00021887	00010000	FC830000	2AC1FFFF	FFFFFFFF	00430005	00A80420	00A90131	1FEA1C65
(280)	1D531E2F	1D4707DA	0014FFFF	FFFF000A	18E00001	00160347	000D1D43	0CE7004E	02CA0057	0004000C
(320)	023B00C9	01282040	1C1E1CFD	1E751D4E	03F20014	007B0005	0003191B	00010000	FE0E0000	2B9F0BB8
(360)	00550296	006A0004	00DFFF81	007D0117	20B31BC0	1C891ED1	1D5807DA	0014FFFF	FFFF0000	19730001
(400)	00230223	00131567	0C180073	030D007C	00040074	015F0031	00FF2126	1B621C15	1F291D62	03F20014
(440)	FFFFFFFF	000019CC	00010000	FCBB0000	2D301035	00860391	008E0004	00C3FF77	008A00DA	21971B04
(480)	1BA11F7C	1D6D07DA	0014FFFF	FFFF0000	1A250001	002902BD	00151844	0C49009C	032400A1	0006011A
(520)	01580085	00982206	1AA51B2D	1EC81D76	03F20014	FFFFFFFF	00001A7D	00010000	FD730000	2BD90BCE
(560)	009502FA	00B30007	00B10095	00870009	226D1A47	1AB9200C	1D8007DA	0014FFFF	FFFF0000	1AB80001
(600)	00260173	00121638	0E830082	039400C5	00030123	FEBA00A7	0D2122A9	1A001A62	20381D88	03F20014
(640)	09250015	00021B10	00010000	FC260000	2D180ABD	00A202F4	00D70005	009BFDFE	008A0AF1	22AA19A1
(680)	19ED2066	1D9107DA	0014FFFF	FFFF0000	1B680001	00210395	002016F4	09DE00D5	02E400EA	00050019
(720)	FF7800A0	09C22256	19431978	20841D9C	03F20014	04F4001D	00021BC0	00010000	FD2C0000	2BCB0B4B
(760)	00E90354	00FC0008	00D2009A	0072094D	21EB18E4	1903208F	1DA607DA	0014FFFF	FFFF0000	1C180001
(800)	001A0519	002615BD	FFFFFFFF	FFFF010D	00030035	FF5300AE	09142179	1886188E	20851DB0	03F20014
(840)	02A40019	000D1C52	00010000	FEAE0000	2C99FFFF	FFFFFFFF	01200005	0059006C	00DC08E2	21051828
(880)	18192068	1DBA07DA	0014FFFF	FFFF000A	1CAA0001	00230317	00241947	0AD100C8	03210134	000801AB
(920)	0441008E	08E120AD	17E117C1	20461DC2	03F20014	03AE001C	00031D02	00010000	FD020000	2E130D5A
(960)	00C3038F	01460007	006E0095	008C08D0	20361783	174B200C	1DCC07DA	0014FFFF	FFFF0000	1D5A0001
(1000)	0014064B	001617EA	FFFFFFFF	FFFF0156	0004017F	FCF700D3	08C41FBF	172616D5	1EC41DD6	03F20014
(1040)	02BE000F	000C1DB1	00010000	FE400000	2C9809DE	00AC02AF	016B0005	00FB00F2	006F08BA	1F4716C8
(1080)	165E1E73	1DDE07DA	0014FFFF	FFFE0000	1DEB0001	001E0E98	00211750	1CA9011E	0721017E	00040165
(1120)	0319006F	08B21ECE	166B15E9	1F1A1DEA	03F20014	008D000C	000D1E43	00010000	FC560000	2DFFFFFF
(1160)	FFFFFFFF	018D0003	0162FEBB	00C808AD	1E731626	15911ED3	1DF107DA	0014FFFF	FFFF000A	1E9A0001
(1200)	001003DE	00321670	0AFC011B	033D01A2	000300F9	FF2E0068	08A71DFA	15CA151B	1E6F1DFB	03F20014
(1240)	01B0001B	00031EF1	00010000	FDB30000	2A6711E7	0173050F	01B50004	02220110	011C08A2	1D80156E
(1280)	14A41E07	1E0407DA	0014FFFF	FFFF0000	1F2C0001	00090544	00131854	FFFFFFFF	FFFF01C4	0002001D
(1320)	27100007	089E1D06	1513142E	1D9B1E0F	03F20014	01E1000B	000D1E83	00010000	FFDE0000	2D7E0A4E
(1360)	00B502D8	01D90002	002B0819	001B089A	1C8C14B8	13B71D2C	1E1807DA	0014FFFF	FFFF0000	1FDA0001
(1400)	000D03FA	00201758	0A2100D7	030201EB	000200DB	FA560010	08971C11	145E1340	1CBA1E22	03F20014
(1440)	02690014	00032118	00010000	FBD70000	2EAC0ADB	010B0336	01FD0002	0327FC4A	002E0894	1BB5141B
(1480)	12E71C64	1E2907DA	0014FFFF	FFFF0000	21C50001	000D000B	002F15EA	09E2012C	0304020F	00020345
(1520)	FBF30016	08911B39	13C21270	1BEE1E33	03F20014	029B001F	0003221C	00010000	FE4D0000	2AF00932
(1560)	014A02D8	02220002	03EFFEAF	0024088F	1ABE136A	11E81B78	1E3C07DA	0014FFFF	FFFF0000	22560001
(1600)	00220F79	004B15BD	0A0801A3	03250234	000402ED	04980047	088C1A42	13131182	1AFF1E46	03F20014
(1640)	02700031	000322AC	00010000	FA830000	2C3C0A85	01B90352	02460004	0413D8F0	0017088A	19C512BC
(1680)	110A1A86	1E4E07DA	0014FFFF	FFFF0000	23020001	00140E54	0056162E	091001A6	02E70259	0003041A
(1720)	0F010018	08871949	12671092	1A0B1E57	03F20014	01C10030	00032357	00010000	FBEC0000	2A6A0A10
(1760)	01F30325	026C0002	04A4F530	00210886	18EB1227	103819AF	1E5F07DA	0014FFFF	FFFF0000	23910001
(1800)	00270E8A	006815A7	0AAA0246	035C027E	0003042E	DA3E001D	0884186E	11D30EC1	19331E68	03E20014
(1840)	01D8003C	000323E7	00010000	FDC6007C	2AFA0A31	024B0337	02910004	0437F395	001BC882	17F01180
(1880)	0F4918B6	1E7007DA	0014FFFF	FFFE0000	243D0001	00360EB5	0089154B	0A3DFFFF	033802A3	000303BE
(1920)	1C2D001F	08801773	112E0ED1	18381E79	03F20014	02DB0063	00032493	00010000	FBE0008B	17FA0A77
(1960)	FFFF035F	02B50003	0398DA1A	001D087E	16F510DD	0E5817BB	1E8207DA	0014FFFF	FFFF0000	24CC0001
(2000)	00490F45	00A21595	0A1CFFFF	033702C7	000403B1	08680019	087D1696	10A10DFE	175B1E88	03F20014
(2040)	01870056	00032523	00010000	FC9300B1	15E009DE	FFFF0335	02DA0002	030B0A94	001D087C	16171052
(2080)	0D8616DD	1E9107DA	00140145	00570003	25790001	002F0E07	00B51581	0AA0FFFF	035202EC	000202C9
(2120)	0AE1001E	087A1598	10050D0D	165E1E99	03F20014	01A80063	000325CE	00010000	FB5000BE	13000AE1
(2160)	FFFF03DC	02FE0003	01901A88	002F0878	15190FB9	0C9515E1	1EA107DA	00140091	004C0001	26400001
(2200)	00450ED8	00D0162E	0A51FFFF	032E0311	00030246	D8F0001C	0877149A	0E6E0C1D	15611EA9	03F20014
(2240)	0315009D	000326CF	00010000	FC5B00E4	16110A83	FFFF0320	03230003	0197D8F0	001A0875	141A0F24
(2280)	0BA414E1	1EB107DA	0014027F	009B0003	27410001	006A0F25	00E815C2	0B79FFFF	03460335	00020125

(12880)	3B2108C0	1B7A07DA	000DFFFF	FFFF000A	239F0001	019500B4	00051738	FFFFFFFF	FFFF126B	000DC053
(12920)	10020002	00BA0384	2D613AB5	08C01B7C	03F2000D	FFFFFFFF	000A2364	000101FF	013E0000	2C41FFFF
(12960)	FFFFFFFF	127D000D	00591665	000200B9	03EA2D4B	3A4908C0	1B7F07DA	000DFFFF	FFFF000A	230C0001
(13000)	019500DA	000524E2	FFFFFFFF	FFFF1290	000C0067	D8F00002	00B80451	2D3339DC	08C01B81	03F2000D
(13040)	FFFFFFFF	000A22B3	00010204	00D90000	2A28FFFF	FFFFFFFF	12A2000C	006AD8F0	000200B8	049E2D20
(13080)	398B08FA	1B8307DA	000DFFFF	FFFE000A	225A0001	01950229	00051FA3	0977002D	015312B5	000C002A
(13120)	D8F00008	00B60504	2D05391E	08FA1B86	03F2000D	FFFFFFFF	00002200	000102CB	01200000	2B98FFFF
(13160)	FFFFFFFF	12C6000C	0061DB60	000200B5	056B2CE9	38B108FA	1B8807DA	000DFFFF	FFFF000A	21C50001
(13200)	01950086	000526F9	FFFFFFFF	FFFF12D9	000C006B	EC730002	00B405D2	2CCB3845	09331B8C	03F2000D
(13240)	FFFFFFFF	000A216B	000101C0	00A60000	2943FFFF	FFFFFFFF	12EB000C	0069F3A4	000200B3	06392CAC
(13280)	37D70933	1B8F07DA	000DFFFF	FFFF000A	21120001	01950139	000522C6	FFFFFFFF	FFFF12FD	000D0061
(13320)	F5B80002	00B30686	2C933786	09691B91	03F2000D	FFFFFFFF	000A20B8	00010214	00F90000	2C2EFFFF
(13360)	FFFFFFFF	13100000	005BF535	000300B2	06EE2C71	37190969	1B9507DA	000DFFFF	FFFF000A	205E0001
(13400)	019500D3	00041D1F	FFFFFFFF	FFFF1322	000C0061	F6690002	00B10755	2C4E36AC	099D1B99	03F2000D
(13440)	FFFFFFFF	000A2005	000101A1	01820000	2C0AFFFF	FFFFFFFF	1334000D	005AF431	000200B0	07BD2C29
(13480)	363F09D0	1B9C07DA	000DFFFF	FFFF000A	1FC90001	01950171	00051677	FFFFFFFF	FFFF1348	000D0056
(13520)	ECF40002	00AF0824	2C0335D2	0A021BA1	03F2000D	FFFFFFFF	000A1F6F	00010204	00CC0000	2996FFFF
(13560)	FFFFFFFF	135A000D	005CD8F0	000200AE	088C2BDB	35640A60	1BA507DA	000DFFFF	FFFF000A	1E150001
(13600)	01930095	00061C27	07160029	0123136C	000D005C	27100002	00AD08D9	2BBC3512	0A8D1BA8	03F2000D
(13640)	FFFFFFFF	00001EBB	000101C4	03890000	2D0CFFFF	FFFFFFFF	137E000D	003E16CD	000500AC	09412B92
(13680)	34A40AB9	1BAC07DA	000DFFFF	FFFF000A	1E610001	01950137	0004163E	FFFFFFFF	FFFF1391	000D0053
(13720)	11CA0002	00AB09A9	2B663436	0B0E1BB1	03F2000D	FFFFFFFF	000A1E07	000101C0	00870000	2986FFFF
(13760)	FFFFFFFF	13A3000D	005808FB	000200AA	0A112B39	33C80B5E	1BB507DA	000DFFFF	FFFF000A	1DCB0001
(13800)	017D0278	00051950	0909002A	015413B5	000C0059	093D0002	00A90A7A	2B0B335B	0B851BBA	03F2000D
(13840)	FFFFFFFF	00001D70	000101CF	02070000	2ACF0998	002C016D	13C9000C	006A0B4C	000300A8	0AE22ADB
(13880)	32ED0BF4	1BC007DA	000DFFFF	FFFF0000	1D150001	0195010C	00051582	FFFFFFFF	FFFF13DA	000C001C
(13920)	D8F00007	00A70B30	2AB6329A	0C181BC3	03F2000D	FFFFFFFF	000A1CBB	0001014A	00380000	2C03FFFF
(13960)	FFFFFFFF	13EC000C	00611DE5	000300A6	0B992A84	322C0C7E	1BC807DA	000DFFFF	FFFF000A	1C610001
(14000)	018E024B	00052380	0BC80029	01AE1400	000C005D	08440003	00A50C02	2A5031BE	0CBF1BCE	03F2000D
(14040)	FFFFFFFF	00001C06	000101A7	01D00000	2AD10E35	002801B9	1412000C	006E0677	000400A3	0C6B2A1B
(14080)	314F0D1B	1BD307DA	000DFFFF	FFFF0000	1BAB0001	019300CC	00051509	0D120024	01951424	000B0066
(14120)	06E40004	00A20CD4	29E430E1	0D731BD9	03F2000D	FFFFFFFF	00001B6F	00010148	02740000	2BFB0F9B
(14160)	002601E5	1436000B	001C0AC9	000900A2	0D2329BB	308E0DC6	1BDD07DA	000DFFFF	FFFF0000	1B140001
(14200)	014C020B	00052074	0B0C001F	01841449	000A0060	1F2E0005	00A00D8C	29823020	0E151BE4	03F2000D
(14240)	FFFFFFFF	00001AB9	0001016A	01E50000	28B3118A	00260221	145B000A	005D1D16	0005009F	0DF62948
(14280)	2FB20E79	1BEA083E	000DFFFF	FFFE0064	1A5E0003	012501BA	00051D9E	10350023	02121460	000A005A
(14320)	09F80004	009E0E5F	290D2F43	0ED71BEF	0456000D	FFFFFFFF	00641A21	0002012D	02E50000	2A1C1078
(14360)	00240223	1481000A	005206E4	0004009D	0ECA28D0	2ED40F45	1BF6083E	000DFFFF	FFFF0064	19C60002
(14400)	01250221	0005219A	0F320020	01F21493	000A0045	04F30006	009C0F34	28932E66	0F971BFC	0456000D
(14440)	FFFFFFFF	0064196A	0002011F	01F80000	2BB31496	00250291	14A50009	0061029A	0004009B	0F832863
(14480)	2E130FE6	1C01083E	000DFFFF	FFFF0064	190F0002	00F603A0	0004131E	12C30020	025614B8	00090050
(14520)	03410003	009A0FEE	28232DA3	10431C08	0456000D	FFFFFFFF	00641883	000200EB	03800000	2A06121A
(14560)	001F024F	14CA0008	006C039E	00040099	105827E2	2D3410AB	1C0F083E	000DFFFF	FFFF0064	18770002
(14600)	00D60206	00002BC7	14050020	027D14DC	0008006F	060B0004	009810C3	27A02CC5	110C1C16	0456000D
(14640)	FFFFFFFF	0064181A	000200C4	02210000	2B5713F7	0021029F	14EE0007	006EE7FF	00040096	112E275C
(14680)	2C561177	1C1D083E	000DFFFF	FFFE0064	17BF0002	00CC0502	00002B8D	15750024	03551502	00070074
(14720)	F00D0003	0095119A	27182BE6	11D91C24	0456000D	FFFFFFFF	00641764	000200D3	036C0000	2C75121C
(14760)	0022027D	15130008	008303F7	00070094	11EA26E3	2B931229	1C2A083E	000DFFFF	FFFE0064	17270002
(14800)	00B80231	00002BC2	138B0025	02CC1525	0007007D	F0160005	00931256	269D2B23	128C1C31	0456000D
(14840)	FFFFFFFF	006416CA	0002							

FILE 1 RECORD 10 5 2158 1973 LENGTH 16850BYTES

(0)	2152000A	0005B7B5	00170015	002909C4	5487FEB5	FC5826DE	0D2F1909	1B820BED	00BF00C5	17510119
(40)	E7A10044	F4AD002E	00000000	FFBD0000	223B1224	00BE03CB	00030005	00940022	00BE04D0	215C2533
(80)	24041E8F	1C2007E1	0003FFFF	FFFF0000	00000001	00220648	00121595	18C400A8	044F0012	00060153
(120)	F2E7009F	04BB210C	25442458	1E4A1C1E	03F90003	02250009	00020001	00010000	02800000	24E81C9F
(160)	00BF04AB	001F0004	018B0076	005F04AB	20BC2555	24AD1E05	1C1C07E1	0003FFFF	FFFF0000	70000001
(200)	001D05BF	00151553	0F5600B4	032D002D	00060121	FF970060	049F206C	25642501	1DC01C1B	03F90003
(240)	05820012	00020320	00010000	01FB0000	20E711BB	008E037A	003A0006	00F80040	010A0498	2037256F
(280)	253A1D92	1C1A07E1	0003FFFF	FFFF0000	C0020001	00000529	00002151	0E580067	02EE008D	000201CD
(320)	009B0022	04731E53	25B92736	1BF01C12	07DC0003	FFFFFFFF	00008000	0001001D	0529000E	14C61099
(360)	00680317	00990003	01C4004D	00130470	1E1D25C0	276E1BC1	1C1103F4	0003022A	00070002	00000001
(400)	000003BD	0000231A	0F4C0064	02F700A7	000301E0	00D00018	046D1DCC	25C927C3	1B7B1C10	07DC0003
(440)	FFFFFFFF	00000001	0001001A	04E2000F	13B40E47	006602E6	00B40003	0217FB0B	0028046A	1D7C25D1
(480)	28171B35	1C0F03F4	00030312	00090002	00000001	00000162	00001B25	11390067	03C700C2	000201F3
(520)	0160000E	04671D2B	25D8286C	1AEE1C0F	07DC0003	FFFFFFFF	00000001	00010013	0672000E	13DC0FCA

ESRO-4 GEOPHYSICAL DATA MAGNETIC MASTER TAPE 31 INDEX. RUN ON 12 DEC 1977 AT 23HR 47MIN (F4M315)

72-092A-01A

D-30957

DSC #420

RECORD	ORBIT	DATE	TIME HR MN SC	ACF1 MV	ACF2 MV	+6V MV	PRE X10	-6V MV	PACK X10	BIAS MV	ACF3 MV	NO. SWEEPS	FEET WRITTEN
1	2	22 NOV 1972	1 42 5	196	204	5939	318	-6239	229	-2830	43	297	0.8
2	3	22 NOV 1972	3 13 43	196	206	5968	406	-6239	221	-2830	43	297	1.6
3	4	22 NOV 1972	4 57 51	196	204	5939	406	-6239	211	-2839	43	394	2.5
4	6	22 NOV 1972	8 30 1	196	202	5939	384	-6239	198	-2830	42	280	3.2
5	7	22 NOV 1972	10 0 54	196	202	5969	384	-6239	195	-2859	43	231	4.0
6	8	22 NOV 1972	11 43 23	196	202	5969	375	-6239	185	-2859	43	315	4.8
7	9	22 NOV 1972	13 24 6	196	202	5969	375	-6239	185	-2859	40	303	5.7
8	10	22 NOV 1972	15 6 6	196	202	5969	375	-6239	181	-2859	42	306	6.5
9	11	22 NOV 1972	16 42 25	196	202	5969	370	-6239	181	-2859	42	195	7.1
10	13	22 NOV 1972	20 30 28	196	201	5969	436	-6239	171	-2859	43	187	7.6
11	14	22 NOV 1972	21 33 4	196	202	5969	370	-6239	185	-2859	43	280	8.4
12	14	22 NOV 1972	21 44 2	196	210	5969	362	-6239	171	-2859	52	259	9.1
13	15	22 NOV 1972	23 10 7	196	202	5969	375	-6239	188	-2859	42	304	10.0
14	16	23 NOV 1972	0 48 26	196	202	5969	375	-6239	185	-2859	42	305	10.8
15	17	23 NOV 1972	2 26 7	10	341	-10437	-15	7649	-15	3299	26	1	10.9
16	18	23 NOV 1972	3 38 12	10	341	-10437	-15	7649	-15	3299	26	1	10.9
17	19	23 NOV 1972	5 45 38	10	341	-10437	-15	7640	-15	3299	26	1	11.0
18	20	23 NOV 1972	7 27 48	196	201	5969	357	-6239	168	-2859	43	287	11.8
19	21	23 NOV 1972	9 9 14	196	201	5969	354	-6239	175	-2859	42	293	12.6
20	22	23 NOV 1972	10 47 5	196	202	5969	350	-6239	175	-2859	42	270	13.4
21	23	23 NOV 1972	12 18 7	196	202	5969	384	-6239	191	-2859	42	248	14.1
22	24	23 NOV 1972	14 0 17	196	202	5969	362	-6239	178	-2859	43	352	15.0
23	25	23 NOV 1972	15 54 36	196	201	5969	350	-6239	161	-2859	43	277	15.8
24	26	23 NOV 1972	17 26 41	196	201	5969	346	-6239	168	-2859	40	290	16.6
25	27	23 NOV 1972	19 5 0	196	201	5969	341	-6239	168	-2859	42	290	17.4
26	28	23 NOV 1972	20 42 51	196	201	5969	341	-6239	168	-2859	43	295	18.3
27	29	23 NOV 1972	22 20 41	196	201	5969	341	-6239	168	-2859	45	292	19.1
28	30	23 NOV 1972	23 58 37	173	183	5969	346	-6239	171	-2859	43	295	19.9
29	31	24 NOV 1972	1 32 3	196	202	5969	362	-6239	175	-2859	42	298	21.0
30	32	24 NOV 1972	3 5 6	196	202	5969	406	-6239	175	-6779	43	309	21.8
31	33	24 NOV 1972	4 44 47	196	202	5969	397	-6239	175	-2859	42	330	22.8
32	34	24 NOV 1972	6 17 1	196	201	5969	344	-6239	158	-2859	42	286	23.5
33	36	24 NOV 1972	9 39 16	196	201	5969	415	-6239	171	-2859	42	352	24.5
34	37	24 NOV 1972	11 33 6	196	201	5969	325	-6239	158	-2859	42	283	25.3
35	38	24 NOV 1972	13 4 9	196	201	5969	362	-6239	168	-2859	40	244	26.2
36	39	24 NOV 1972	14 54 9	196	201	5969	375	-6239	151	-2859	42	325	27.1
37	40	24 NOV 1972	16 40 14	195	201	5969	339	-6239	141	-2859	41	216	27.7
38	41	24 NOV 1972	18 10 42	196	201	5969	321	-6239	161	-2859	44	298	28.4
39	44	24 NOV 1972	23 3 50	200	201	5969	321	-6239	155	-2859	44	258	29.1
40	45	25 NOV 1972	0 40 57	173	181	5969	325	-6239	155	-2859	30	291	29.9
41	46	25 NOV 1972	2 16 4	196	201	5969	350	-6239	161	-2859	42	402	31.0
42	46	25 NOV 1972	3 1 36	195	201	5969	411	-6239	138	-2879	51	187	31.6
43	47	25 NOV 1972	3 51 16	195	201	5969	375	-6239	161	-6779	43	329	32.5
44	49	25 NOV 1972	7 9 17	195	201	5969	375	-6239	158	-2859	41	433	33.4
45	50	25 NOV 1972	9 8 10	195	200	5969	314	-6239	135	-2879	41	265	34.1
46	51	25 NOV 1972	10 38 0	195	201	5969	314	-6239	145	-2859	43	296	34.9
47	53	25 NOV 1972	13 50 34	195	201	5969	329	-6239	151	-2859	46	254	35.6
48	54	25 NOV 1972	15 28 43	195	201	5969	333	-6239	151	-2859	43	332	36.5
49	55	25 NOV 1972	17 16 58	195	201	5969	307	-6239	138	-2879	38	298	37.4
50	56	25 NOV 1972	18 54 58	195	200	5969	303	-6239	138	-2879	38	274	38.1
51	57	25 NOV 1972	20 33 8	195	200	5969	307	-6239	138	-2879	41	294	39.0
52	58	25 NOV 1972	22 10 29	195	201	5969	303	-6239	141	-2879	41	300	39.8
53	59	26 NOV 1972	0 27 17	195	200	5969	307	-6239	135	-2879	41	177	40.3
54	60	26 NOV 1972	1 26 34	195	200	5969	307	-6239	141	-2859	41	289	41.1
55	61	26 NOV 1972	3 1 56	195	201	5969	321	-6239	148	-2859	41	319	42.0
56	62	26 NOV 1972	4 43 8	195	200	5969	325	-6239	138	-2879	41	307	42.8